

**TERRESTRIAL-AQUATIC TRANSFERS OF CARBON DIOXIDE, METHANE, AND
ORGANIC CARBON FROM RIPARIAN WETLANDS TO AN ARCTIC HEADWATER
STREAM**

Benjamin Lloyd Miller

A thesis submitted to the faculty of the University of Michigan at Ann Arbor, Rackham Graduate School of Literature, Arts, and Sciences in partial fulfillment of the requirements for the degree of Traditional Master of Science in the Department of Ecology and Evolutionary Biology.

Ann Arbor

2014

Approved by:

George W. Kling

Knute J. Nadelhoffer

Bethany T. Neilson

CONTENTS

1.0	Abstract.....	3
2.0	Acknowledgements.....	5
3.0	Introduction.....	6
4.0	Methods.....	9
5.0	Results.....	25
6.0	Discussion.....	50
7.0	Conclusions.....	55
8.0	References.....	56
9.0	Appendix A.....	66
10.0	Appendix B.....	68
11.0	Appendix C.....	70
12.0	Appendix D.....	73
13.0	Appendix E.....	78
14.0	Appendix F.....	83

1.0 ABSTRACT

BENJAMIN L. MILLER: Terrestrial-aquatic Transfers of Carbon Dioxide, Methane, and Organic Carbon From Riparian Wetlands to an Arctic Headwater Stream
(Under the direction of George W. Kling)

Transfers of dissolved gases from land contribute to gas evasion from surface waters. Although headwater streams may contribute strongly to overall gas evasion in a river network, the dynamics of CO₂ and CH₄ transfers between riparian wetlands and headwater streams are poorly understood. Imnavait Creek, a peat-bottom, beaded arctic headwater stream, was studied to determine the relative importance of CO₂, CH₄, and dissolved organic carbon (DOC) fluxes from surface inflow, in-stream processing such as photo-mineralization, and subsurface lateral inflows draining riparian wetland soils at different depths. Although concentrations of CO₂ and CH₄ were 1-2 orders of magnitude higher in subsurface lateral inflows than in surface waters, subsurface discharge was >0.1% of surface discharge along the studied reach of Imnavait. This means that 91-97% of the C entering and leaving this reach was introduced by surface inflows. Integrating the subsurface inflows per meter of stream reach above the study site provided the distances required to account for surface water concentrations at the upstream entry to the study reach. Assuming that subsurface inflows were similar along the entire stream, these distances were 120-363 m for CO₂, 41-47 m for CH₄, and 36 m for DOC. All of these distances were much less than the distance to Imnavait's headwater source (~430 m), implying a loss of gases through evasion to the atmosphere and a loss of DOC through photochemical or biological conversion to CO₂ from upstream to downstream. Furthermore, concentrations of CO₂ were significantly higher upstream (p=0.02), while CH₄ concentrations were significantly higher downstream (p<0.001). CO₂ evasion from the surface of Imnavait pools was 14-30% of the CO₂ imported within subsurface lateral inflows, while CH₄ evasion was only 4-6%. Both CO₂ and CH₄ evasion increased significantly during periods of thermal stratification in the pools (p<0.001 and p=0.02, respectively), when concentrations of these

gases increased in bottom waters influenced primarily by C-rich subsurface lateral inflows. Photo-mineralization of aromatic DOC from subsurface lateral inflows further increased CO₂ in Imnavait. Deeper subsurface lateral inflows (10 cm depth to the permafrost boundary) tended to have significantly higher CO₂ and CH₄ concentrations than shallow subsurface lateral inflows (0 to 10 cm depth). Deeper subsurface lateral inflows of C-rich soil water to Imnavait increased over the summer proportionately with thaw depth. Current scenarios of global change for Alaska's North Slope indicate that while terrestrial-aquatic C transfers via subsurface lateral inflows of soil water may increase in the future, in-stream stratification and thus greater gas evasion may decrease.

2.0 ACKNOWLEDGEMENTS

This material is based upon work supported by the National Science Foundation (NSF) Graduate Research Fellowship under Grant No. DGE 1256260. User days at Toolik Field Station and equipment were funded by research grants through the University of Michigan, Department of Ecology and Evolutionary Biology, NSF-ARC 1107707, NSF-DEB 1026843, NSF-OPP 1022876/1023270, and NSF 1204220. Special thanks to Tyler King, Sara Fortin, Jonathan Celmer, and Colleen Peters for help collecting samples, to Tyler King, Anna Clinger and Susanna Michael for help analyzing samples, to Kevin Befus for GPS coordinates, and to Katherine Harrold and Knute Nadelhoffer for helpful comments on this manuscript. Final submission of this thesis for publication will include George W. Kling and Bethany T. Neilson as co-authors.

3.0 INTRODUCTION

Headwater streams comprise half the length (Knighton, 1998) and a large proportion of surface area in any river network (Butman and Raymond, 2011). A recent global synthesis by Raymond et al. (2013) showed that headwater streams have higher carbon dioxide (CO₂) concentrations and greater evasion to the atmosphere than lakes and larger rivers. These findings are consistent with other studies (Jones and Mulholland, 1998; Hope et al., 2001; Neu and Krusche, 2011; Butman and Raymond, 2011), which found that CO₂ concentrations increase as stream order decreases. Higher sediment surface area to water volume ratios, steeper elevation gradients resulting in stream velocities that increase gas exchange through eddy diffusion (Raymond et al., 2012), and higher CO₂ concentrations upstream than downstream (Crawford et al., 2013) indicate that headwater streams may serve as a “conduit” for CO₂ from soil water to the atmosphere. Measurements focused on lakes and larger rivers could therefore miss terrestrial-aquatic carbon (C) transfers and underestimate CO₂ evasion from inland waters. Higher CO₂ concentrations upstream than downstream have also been documented within boreal headwater streams (Jonsson et al., 2007; Teodoru et al., 2009; Humborg et al., 2010; Crawford et al., 2013). However, no studies have directly measured the magnitude of CO₂ flowing into arctic headwater streams within soil water, or the resulting impact on in-stream CO₂ concentrations and evasion to the atmosphere.

Terrestrial-aquatic C transfers to headwater streams in the Arctic also include dissolved organic C (DOC) (Peterson et al., 1986; Judd and Kling, 2002) and the products of its anaerobic oxidation by the microbial community, CO₂ and CH₄. Continuous permafrost in the Arctic confines the infiltration of soil water to lateral flow paths across the permafrost boundary, through shallow peat soils (Hinzman et

al., 1991). Organic C dissolving from saturated peat into soil water may be oxidized to CO₂ and CH₄ by microbes (Martineau et al., 2014). Historically, primary production in the arctic has been greater than respiration, leaving peat deposits that contain large amounts of incompletely oxidized organic C (McGuire et al., 2009). Today, permafrost soils contain 1,600 Pg or 50% of the subsurface terrestrial C pool (Tarnocai et al., 2009). As permafrost thaws, more of this stored C will become active in the global C cycle. Conduits that will link the subsurface terrestrial C pool to aquatic C pools (e.g., lakes and oceans; Kling et al., 1991) may include subsurface lateral inflows of soil water to headwater streams and larger rivers.

The extent to which DOC, CO₂, and CH₄ dissolve into soil water is governed by the amount of time this water resides in the subsurface. Longer water residence times within the subsurface typically result in higher solute concentrations (Mulholland, 1993). Water residence times within the hyporheic zone (Zarnetske et al., 2007) and riparian wetlands (Merck et al., 2012) have been shown to be important to in-stream concentrations of DOC and other solutes throughout the ice-free season within arctic headwater streams. An important characteristic of peat soils in the arctic that affects water residence times is its tendency to compact at greater subsurface depths (Clymo, 1984). As peat compacts, its porosity is reduced (Clymo, 1984), decreasing hydraulic conductivity (Hinzman et al., 1991) and forcing subsurface lateral inflows of soil water along a more tortuous path to headwater streams or larger rivers. This more tortuous path results in longer water residence times and—potentially—higher concentrations of DOC, CO₂, and CH₄ within deeper subsurface lateral inflows.

At the interface between land and water, the low topographic position of riparian wetlands makes them perennially saturated collection areas for terrestrial runoff. In lower latitude wetlands, DOC is

commonly exported from wetlands to surface waters (Schiff et al., 1998; Freeman et al., 2004). Though studies have also demonstrated the evasion CH_4 from wetlands to the atmosphere (Christensen, 1993; Altor and Mitsch, 2006), none have directly measured the magnitude of CH_4 flowing into arctic headwater streams from wetlands, or the resulting impact on in-stream CH_4 concentrations and evasion.

Once in surface waters, DOC and CH_4 may undergo further oxidation—or mineralization—by microbes (Crump et al., 2003), sunlight (i.e., photo-mineralization; Cory et al., 2013), and hydroxyl radical ($\bullet\text{OH}$; Page et al., 2013). These fates of terrestrially derived DOC and CH_4 are influenced by in-stream water residence times, which are influenced by stratification. The pools of Innavait Creek, an arctic headwater stream, are known to thermally stratify (Irons and Oswood, 1992; Merck et al., 2012). Merck et al. (2012) showed that the chemical character of DOC compounds in the bottom waters of Innavait pools closely resembled DOC from subsurface soil waters. Thus, the division of these pools into surface waters influenced by surface inflow and bottom waters influenced by subsurface lateral inflows, may allow for separate water residence times and rates of DOC and CH_4 alteration by in-stream oxidation.

For this study, we determined the magnitude of terrestrial-aquatic C transfers from riparian wetlands to an arctic headwater stream, and the resulting impacts to stream C chemistry. We determined the magnitude of terrestrial-aquatic C transfers by measuring subsurface lateral inflows of soil water and their C content draining riparian wetlands at different depths. Contributions of surface water inflow, in-stream processing of DOC, and wetland processing of DOC to the C observed leaving a defined reach of Innavait Creek were also measured. We then determined the relative importance of terrestrial-aquatic C transfers, surface inflows, and in-stream processing to CO_2 and CH_4 saturation in Innavait Creek using a

mass balance approach. Here, we were primarily concerned with the gaseous products of DOC oxidation, the greenhouse gases CO₂ and CH₄. In order to explain gas concentrations in water, residence times in subsurface soils and the physical process affecting in-stream water residence times, thermal stratification, were also measured. Additionally, we measured the chemical character of DOM compounds, and thus their susceptibility to different forms of oxidation. We show that terrestrial-aquatic transfers of relatively small amounts of CO₂ and CH₄ per m of Innavait contribute to their saturation of surface waters and evasion to the atmosphere. We also show that such terrestrial-aquatic transfers increase with temperature over the summer in the Arctic, which could have implications for scenarios of global change.

4.0 METHODS

4.1 Study Site

Innavait Creek is a first-order tributary of the Kuparuk River located near Toolik Lake in Alaska (68.616° N latitude, 149.318° E longitude, ~ 910 m elevation; Figure 1a). Innavait is surrounded by lowland tundra characterized by peat soils with underlying continuous permafrost (Walker et al., 1987). It is one of many beaded streams on the North Slope of the Brooks Mountain Range (Appendix A, Figure A1) (Merck et al., 2012). Beaded streams result from the thermal erosion of subsurface ice masses by surface streams, and subsequent collapse of surrounding channel morphology into a series of pools, or “beads” (McNamara et al., 1998). The upper Innavait Creek basin (2.2 km²) has a mean of 13 pools per 100 m, which range from 1 to 323 m² in surface area and from 0.1 to 2.7 m in depth (Merck et al., 2012). Surface pools are connected by chutes (Figure 1b). The riparian zone is characterized by wet

sedge tundra (Figure 1c; Appendix A, Figure A2). This study was conducted from June 20 to August 6, 2013, focused on a 14.5 m stream reach of encompassing two main surface pools, and included a downstream chute, Imnavait Weir (Figure 1).

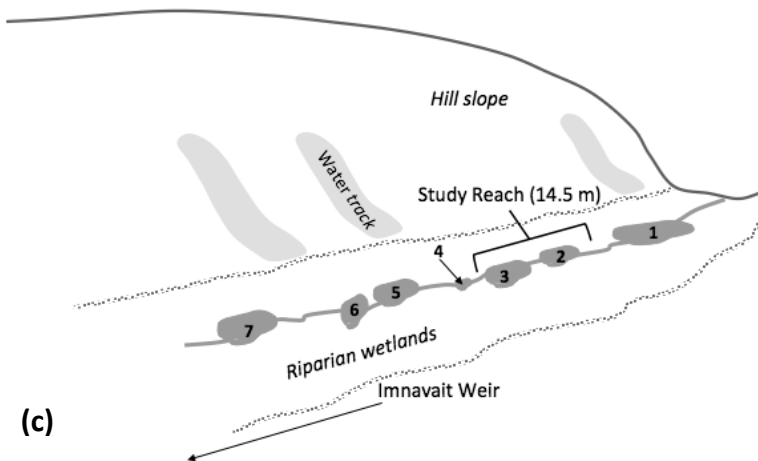
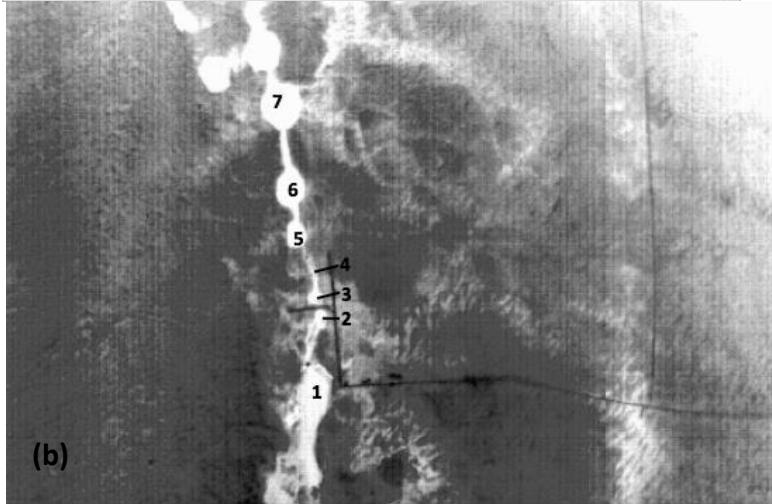
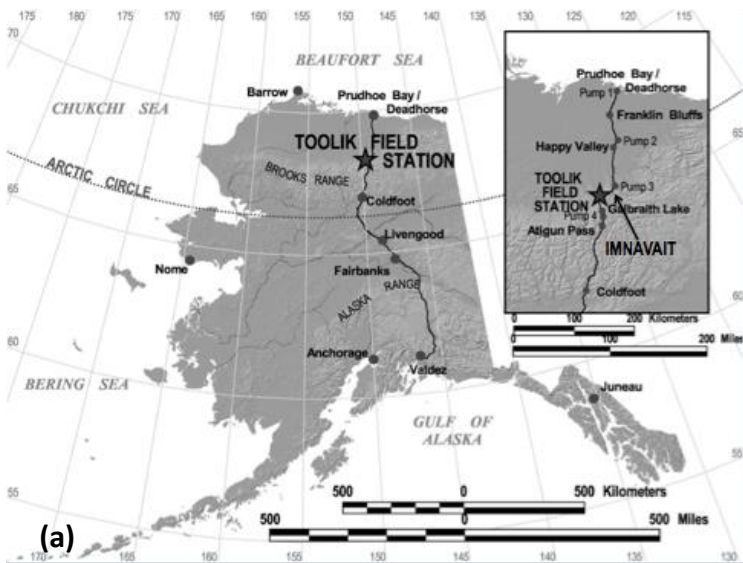


Figure 1. (a) Imnavait Creek was accessed from Toolik Field Station on the North Slope of Alaska. Thermal imaging (b) displays the inflows, outflows, and general hydraulic connectivity of Imnavait

pools in white. The Imnavait study reach (c) encompasses two pools in a valley with riparian wet sedge tundra, ~0.7 km upstream from Imnavait Weir.

4.2 Water Balance

The water balance of a defined reach of Innavait Creek during its ice-free season was represented as:

$$\frac{dV}{dt} = (I_{Surface} + I_{Subsurface} + P) - (O_{Surface} + O_{Subsurface}) - E \quad (1)$$

where dV/dt is the change in volume of water observed over time (1 h), I is the sum of surface water inflow and subsurface lateral inflows, P is precipitation, O is the sum of surface water outflow and subsurface outflow, and E is evaporative loss. All water balance units are in $L h^{-1}$. Water balances were calculated for Pools 2 and 3 individually and combined as a reach on six dates, during July 4, July 5, July 16, July 26, July 31, and August 3, 2013.

Surface inflow—Inflow into Pool 2 was measured using a v-notch flume at the outlet of Pool 1 (Figure 1). The flume was calibrated using measured discharge and a pressure transducer (Level Troll 500, In-Situ Inc.; Appendix B). Surface inflow measured using this method was accurate to $\pm 9\%$. Surface inflow into Pool 3 was estimated by adding surface inflow into Pool 2, precipitation into Pool 2, and subsurface lateral inflows into Pool 2, and then subtracting evaporative loss from Pool 2. Thus, Pool 2 outflow was equal to Pool 3 inflow. Surface flow was also measured downstream of the study reach, at Innavait Weir, using a Marsh McBirney Flo-Mate 2000 velocity meter.

Subsurface lateral inflows—Subsurface lateral inflows perpendicular to Pools 2 and 3 from the east and west riparian wetlands were estimated using differences between water elevations within piezometers installed in the wetlands and surface water elevations of Pools 2 and 3, according to Darcy's Law (Figure 2; Appendix B). Stage height was measured both manually and by using Aqua Troll 200 (In-Situ Inc.) pressure transducers. Water elevation in each piezometer was then determined by GPS (Trimble S3 Servo-Autolock-Robotic Total Station). Pool stage heights were measured continuously (600LS pressure transducer, YSI) from June 26 and pool water elevations were determined by GPS in Pools 2 and 3 on August 3. This relationship between continuous pressure measurements and surface water elevation was used to extrapolate pool water elevation from stage height on other dates.

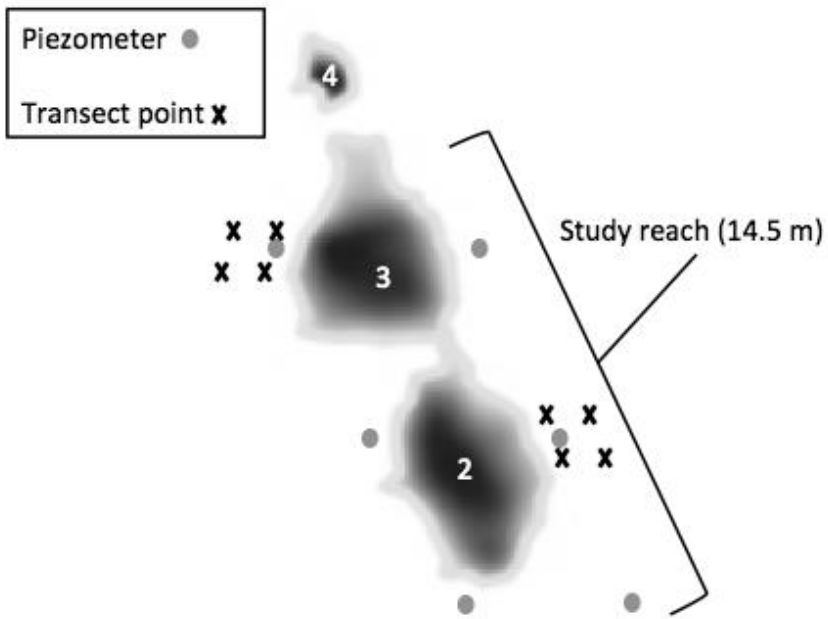


Figure 2. Innavaik study reach. Positions of piezometers and transect points in riparian wetlands relative to each pool are marked.

Hydraulic conductivities measured using falling head tests in riparian wetlands decreased from 0.004 cm s^{-1} at 10 cm depth to 0.002 cm s^{-1} at 25 cm depth. Therefore, subsurface lateral inflows to Imnavait were estimated separately for (1) 0 to 10 cm and for (2) 10 cm to the base of the active layer. The latter expanded with thaw depth over the study period. It is important to note that the heterogeneity of hydraulic conductivities, the presence or absence of preferential flow paths, and the actual area of soil through which subsurface water flows each contributed unquantifiable but sizeable uncertainty to the method used to estimate subsurface lateral inflows. Subsurface lateral inflows were estimated for 0 to 10 cm depth and for 10 cm depth to the permafrost boundary adjacent to the Pool 2 and Pool 3 piezometers in the east and west riparian wetlands (Figure 2), for a total of eight subsurface lateral inflows ($n=8$) on each of the six dates of the water balances.

The permafrost boundary and thus the volume of the subsurface participating in the water and C mass balances became deeper throughout the summer. This expansion of thaw depth was measured with a steel probe along transects through riparian wetlands during the study period. To determine the approximate time subsurface water interacted with peat on the dates of the water balances, residence time, τ (d), was estimated as:

$$\tau = \frac{V}{Q} \quad (2)$$

where V is the volume of subsurface water underlying riparian wetlands (L), obtained by multiplying surface area (m^2) by mean local thaw depth (m; $\text{m}^3 = 10^3 \text{ L}$) by the porosity of the subsurface (dimensionless ratio), assuming this subsurface pore space is flooded. Separate

subsurface water volumes for 0 to 10 cm depth and for 10 cm depth to the base of the active layer were calculated and divided by subsurface discharge (Q) at these layers to obtain approximate τ . Residence times were thus calculated for 0 to 10 cm depth and for 10 cm depth to the permafrost boundary adjacent to the Pool 2 and Pool 3 piezometers in the east and west riparian wetlands (Figure 2), for a total of eight residence times ($n=8$) on each of the six dates of the water balances.

Surface and subsurface outflows—Surface outflow at the outlet of Pool 3 was obtained by adding surface inflow, precipitation (obtained from NRCS, 2013), and subsurface lateral inflows, and then subtracting evaporative loss. Subsurface outflows, or leakage, out of the pools and back into the riparian zone were assumed to be negligible because piezometer water elevations were consistently greater than pool surface water elevations.

Evaporation—Evaporation, E , was estimated using the aerodynamic method:

$$E = M (v_s - v_{0.5}) u_{0.5} \quad (3)$$

$$M = 0.622 \left(\frac{\rho_a C_E}{\rho_w P} \right) \quad (4)$$

where M is the mass transfer coefficient (kPa^{-1}), v_s is the saturation vapor pressure at mean water temperature (kPa), $v_{0.5}$ is vapor pressure 0.5 m above the pool surface (kPa), assuming a relative humidity of 25%, $u_{0.5}$ is wind speed 0.5 m above the pool surface (m s^{-1}), ρ_a and ρ_w are the temperature-dependent densities of air and water (kg m^{-3}), P is atmospheric pressure at 910 m

(kPa), and C_E is a dimensionless bulk evaporation coefficient, assumed here to be 0.0014 (Gupta, 2001). Wind speed at pool surface was estimated as described in section 4.2.

4.3 C Mass Balances

Concentrations of CO₂, CH₄, and DOC were measured within each surface and subsurface inflow and outflow estimated on July 5, July 26, and August 3, 2013. Concentrations of CO₂ and CH₄ in surface water were sampled with syringes and determined via thermal conductivity and inductively coupled plasma gas chromatography (Shimadzu TCD-FID GC-14A; detailed methods in Kling et al., 2000). DOC and Total Dissolved Nitrogen (TDN) samples were acidified to pH<4 and analyzed on a Shimadzu TOC-V CPH analyzer with a TNM-1 unit. Further characterization of DOC is described in section 4.4. Three, replicate subsurface water samples were collected with syringes attached to stainless steel needles at 0 to 10 cm depth (10 cm) and at 10 cm depth to the permafrost boundary (25 cm) near piezometers installed in the east and west riparian wetlands, for a total of 12 on each date of three dates of the C mass balances ($n=12$) (Figure 2). All inflow and outflow terms in the water balance were multiplied by corresponding concentrations of CO₂, CH₄, and DOC (mg C L⁻¹) to obtain terms for C mass balances, in mg h⁻¹ (Appendix B). Each C mass balance was represented as:

$$\frac{dm}{dt} = m_O - m_{Surface} - m_{Subsurface} - m_{F_h} + m_{F_e} - m_B - m_W - m_P - m_{OH} \quad (5)$$

where dm/dt is the change in mass observed over time (1 h), m_O is the mass of C leaving the study reach from Pool 3, $m_{Surface}$ is the mass of C entering in surface inflow, $m_{Subsurface}$ is the

mass of C entering within subsurface lateral inflows, m_{Fh} is the mass of C entering from the hyporheic zone (pool bottoms), and m_{Fe} is the mass of C leaving from the pool surface (gas evasion).

In-stream mineralization of DOC by microbes attached to benthic sediments (on the pool bottoms; m_H) and by microbes suspended in the water column (m_B) also added CO_2 to the study reach. In addition, estimates for abiotic photomineralization within the water column (m_P ; 110 $\text{mg CO}_2\text{-C m}^{-2} \text{ h}^{-1}$; R. Cory, unpublished) and for abiotic mineralization of DOC by $\bullet\text{OH}$ within the water column (m_{OH} ; $1.5 \times 10^{-5} \text{ mg CO}_2\text{-C L}^{-1} \text{ h}^{-1}$; Page et al., 2013) were included in the $\text{CO}_2\text{-C}$ mass balances. Photo-mineralization estimates were scaled to the surface area of each pool, because high concentrations of DOC in Imnavait Creek have been shown to rapidly attenuate sunlight (R. Cory, unpublished). Mineralization by $\bullet\text{OH}$ was scaled to the volumes of Pools 2 and 3.

Hyporheic flux—Three replicate fluxes of dissolved CO_2 and CH_4 ($\text{mg C m}^{-2} \text{ d}^{-1}$) from the hyporheic zone were estimated near the inflow ($n=3$), middle ($n=3$), and outflow ($n=3$) of Pool 6. Pool 6 was measured to avoid increases in dissolved gases and DOC in surface waters along the study reach that may have resulted from disturbing benthic sediments. Concentration gradients of CO_2 and CH_4 between the hyporheic zone and overlying surface water were measured by syringes attached to stainless steel needles. Hyporheic fluxes of CO_2 and CH_4 , F_h , were then estimated using Fick's Law, porosity (ϕ ; 0.86 for 5 to 10 cm depth) (Hinzman et al., 1991), and tortuosity (θ) (Sweerts, 1991):

$$F_h = -\phi (D_0 \times \theta^{-2}) \frac{dC}{dz} \quad (6)$$

$$\theta^2 = 0.73 \phi + 2.17 \quad (7)$$

where D_0 is a temperature-dependent diffusion coefficient for CO_2 ($1.08 \times 10^{-5} \text{ cm}^2 \text{ s}^{-1}$) or CH_4 ($1.14 \times 10^{-5} \text{ cm}^2 \text{ s}^{-1}$) at 5 °C (Broecker and Peng, 1974), dC / dz is the concentration gradient (mg L^{-1}) measured between the hyporheic zone at depth z and surface water (10 cm) (Berner, 1980; Huttunen et al., 2006). These hyporheic fluxes were estimated during July 3, July 18, and July 29, and assumed to be representative of those in other pools on the dates of the mass balances. Hyporheic fluxes were scaled to the sediment surface areas (m^2), divided into thirds, of Pools 2 and 3 on the dates of the mass balances.

Benthic mineralization—Benthic mineralization was estimated using three 1.5 L opaque chambers with a surface area of 91 cm^2 deployed on the bottom of Pool 4 ($n=3$ replicates). Pool 4 was measured to avoid increases in gases and DOC in surface waters along the study reach that may have resulted from disturbing benthic sediments. Oxygen consumption in the chamber was measured (ProODO, YSI) and related on an equi-molar basis to CO_2 production. The slope of CO_2 production over time per unit area was multiplied by the chamber volume, and the resulting flux ($\text{mg CO}_2\text{-C m}^{-2} \text{ h}^{-1}$) scaled to the sediment surface areas (m^2) of Pools 2 and 3 on the dates of the mass balances. Similar to hyporheic flux estimates, benthic mineralization estimates in Pool 4 during July 31 to August 3 were assumed to be representative of those in other pools on the dates of the mass balances.

Water column mineralization—Mineralization within the water column was also estimated via oxygen consumption measured in 60 mL BOD vials (YSI, ProODO). During the stratification that developed in Pools 2 and 3 on July 15 and August 4, water from the epilimnion ($n=3$ replicates) and hypolimnion ($n=3$ replicates) of each pool was sampled and allowed to equilibrate with the atmosphere for 24 h at 7 °C. During each experiment, 15 μL HgCl_2 were added to three BOD bottles to serve as killed controls. Following a minimum four-day incubation period at 5 °C, rates of oxygen consumption and CO_2 production for each BOD bottle were calculated. Mineralization rates ($\text{g CO}_2\text{-C L}^{-1} \text{h}^{-1}$) were assumed to be representative of those on the dates of the mass balances, and scaled to the volumes and water residence times of Pools 2 and 3 on those dates.

4.4 *Chemical Characterization of DOM*

The susceptibility of DOM to microbial oxidation within surface and subsurface lateral inflows was first assessed by calculating DOC:TDN molar ratios. DOM samples from Imnavait Creek ($n=8$) and from riparian wetlands at 0 to 10 cm depth ($n=8$) and 10 cm depth to the permafrost boundary ($n=8$) were characterized throughout the study period, for a total of 24 samples. Because our sampled DOM originates in oligotrophic and highly reduced wetland environments, we assume that concentrations of NH_4^+ and NO_3^- are low and most TDN was an organic component of DOM. The UV-Visible absorbance spectrum of chromophoric DOM (CDOM) (a_{300} ; $n=24$) was characterized via an Aqualog silicon photodiode detector (Aqualog, Horiba) following Page et al. (2014). The spectral slope ratio (S_R ; $n=24$), or a proxy for the average molecular weight of CDOM, was calculated from the absorbance spectrum of each

sample following Helms et al. (2008). Decadic CDOM absorption coefficients, $dec_{CDOM\lambda}$, were calculated by dividing the measured absorbance by the cuvette pathlength (0.01 m) and multiplying by 2.303. $SUVA_{254}$ was estimated by dividing the decadic absorption coefficient at 254 nm by the concentration of DOC (mg C L^{-1}) ($n=24$; Weishaar et al., 2003).

Fluorescence excitation-emission matrices (EEMs) were measured via an Aqualog (Horiba). EEMs of each sample were collected following Ward et al. (2014). Matlab (version 7.7) was used to correct EEMs for inner-filter effect and instrument-specific excitation and emission corrections following Cory et al. (2010). Fluorescence index (FI ; $n=24$) is the ratio of corrected fluorescence emission intensities at 470 and 520 nm at excitation wavelength 370 nm; this is a proxy for the aromaticity of the fulvic acid fraction of CDOM (McKnight et al., 2001), and was calculated following Cory et al. (2010).

4.5 Wetland Processing

Concentrations of dissolved CO_2 and CH_4 were measured at transect points in riparian wetlands adjacent to Pools 2 and 3 of Innavait Creek during June 26, July 9, and August 1. Adjacent to each pool, two transect points were spaced ~ 2.5 m apart in areas with (wet) and without (dry) standing water located 1 m from the pool edge, while two others were spaced ~ 2.5 m apart in wet and dry areas located 6 m from the pool edge (Figure 2). Soil water was sampled at 0 to 10 cm depth (10 cm; $n=3$ replicates) and at 10 cm depth to the permafrost boundary (25 cm; $n=3$ replicates) as described in section 4.3. Using the data from these transects, each

environment's relative contribution to CO₂ and CH₄ saturation within subsurface lateral inflows was assessed during the study period.

Microbial mineralization and CO₂ production within riparian soils was also measured and compared to CO₂ production within pool sediments, surface waters, and hill slope soils. At each dry riparian transect point, three replicate 1.77 cm³ soil cores were sampled at 0 to 10 cm depth (10 cm; $n=3$) and at 10 cm to the permafrost boundary (25 cm; $n=3$) 1 m and 6 m from the pool edge using a hollow stainless steel tube, for a total of 12 soil cores on three dates, during June 26, July 16, and August 4. Soils at wet riparian transect points were generally unconsolidated and could not be sampled using this method. Three replicate cores of the same dimensions were taken outside of the study reach at two hill slope sites on two dates, during July 17 and August 4, both inside ($n=3$ replicates) and outside of a water track. Hill slope soil cores taken outside of the water track were sampled from both the upper organic ($n=3$ replicates) and lower mineral soil layers ($n=3$ replicates). In addition, three, replicate 10 cm deep sediment cores (volume=3.53 cm³) were taken near the inlet ($n=3$), middle ($n=3$), and outlet ($n=3$) of Pool 6 on two dates, during July 4 and July 23. Cores and subsurface water collected from each site were allowed to equilibrate with ambient oxygen levels for 24 h at 7 °C. Following this, the upper 2 cm of each core was subsampled, wrapped in acid-washed nylon, and placed in a 60 mL BOD bottle along with subsurface water from its corresponding location. CO₂ production rates were measured in $\mu\text{mol L}^{-1} \text{h}^{-1}$ as described in section 4.3 following a minimum four-day incubation period at 7 °C. CO₂ production rates were then normalized to dry weight of incubated cores ($\mu\text{mol CO}_2 \text{L}^{-1} \text{h}^{-1} \text{g}^{-1}$).

4.6 In-stream Gas Concentrations and Evasion

Three replicate dissolved gas samples from the surface of Pools 2 ($n=3$) and 3 ($n=3$) of the study reach were collected with syringes and partial pressures of CO_2 and CH_4 (μatm) were determined as described in section 4.2. The same sampling was carried out at Innavaite Weir, 0.7 km downstream of Pool 3 ($n=2$ replicates). Evasion, F_e , of dissolved CO_2 ($n=3$ replicates) and CH_4 ($n=3$ replicates; $\text{mg C m}^{-2} \text{ h}^{-1}$) from the surface of Pools 2 and 3 to the atmosphere was estimated using in-stream gas partial pressures and the thin boundary-layer equation:

$$F_e = k \times K_H(pGas_w - pGas_a) \quad (8)$$

where k is the gas transfer velocity (cm h^{-1}), $pGas_w$ is the partial pressure of a gas in water (μatm), $pGas_a$ is the partial pressure of a gas in water at equilibrium with ambient air (μatm), and K_H is a water temperature-dependent Henry's constant ($\text{mmol kg}^{-1} \text{ atm}^{-1}$; Wilhelm et al., 1977; Vachon et al., 2010). Water temperatures in Pools 2 and 3 were measured continuously throughout the June 20 to August 6 study period to capture thermal stratification using thermistors (HOBO Water Temp Pro V2) suspended from buoys on chains at 10 cm intervals. Thermistor chains extended from the surface to the bottom of each pool. The gas transfer velocity, k (cm h^{-1}), at wind speeds $< 3.7 \text{ m s}^{-1}$ was determined using the following relationships:

$$k = k_{600} \left(\frac{Sc}{600} \right)^{-0.66} \quad (9)$$

$$Sc = a - bT + cT^2 - dT^3 \quad (10)$$

where Sc is the Schmidt number describing the ratio of viscosity (m s^{-1}) to molecular diffusion (m s^{-1}) at T , T is the water temperature ($^{\circ}\text{C}$), and a , b , c , and d are the dimensionless constants for CO_2 and CH_4 (Wanninkhof, 1992; Crusius and Wanninkhof, 2003). k_{600} (cm h^{-1}) is the gas transfer velocity given at a Schmidt number of 600, which normalizes k for comparison of any gas at any temperature (Bastviken et al., 2004). Although Crusius and Wanninkhof (2003) assume a k_{600} of 1.0 cm h^{-1} at wind speeds $< 3.7 \text{ m s}^{-1}$, k_{600} was also calculated using wind speed following Cole and Caracao (1998):

$$k_{600} = 2.07 + 0.215 (U_{10})^{1.7} \quad (11)$$

where U_{10} is the wind speed at 10 m above the water's surface. Because this relationship does not account for the role of convection, k_{600} was also calculated following MacIntyre et al. (2010) and Schubert et al. (2012). For water cooler than the ambient air temperature:

$$k_{600} = 1.74 (U_{10}) - 0.15 \quad (12)$$

For water warmer than the ambient air temperature:

$$k_{600} = 2.04 (U_{10}) + 2.0 \quad (13)$$

U_{10} was determined using:

$$U_{10} = U_{0.5} \left[1 + \frac{(C_{d10})^{0.5}}{\kappa} \ln \left(\frac{10}{0.5} \right) \right] \quad (14)$$

where $U_{0.5}$ is the wind speed measured 0.5 m above the pool surface (m s^{-1}), C_{d10} is a mean drag coefficient 10 m above the water's surface (dimensionless), and κ is the von Karman constant (0.41; Crusius and Wanninkhof, 2003; Vachon et al., 2010). Wind speed 0.5 m above the pool surface was estimated from a linear regression between anemometer data taken near Pools 2 and 3 during 2013 (NRCS, 2010-2013) and wind speed measured 0.5 m above the surface of Imnavait during 2010 (Campbell Scientific, Model 207). Compared to lakes, the Pools 2 and 3 have a short fetch and are bordered by wet sedge tundra; thus, U_{10} was calculated using two C_{d10} values determined for “frictionless” lakes (1.3×10^{-3} ; Crusius and Wanninkhof, 2003) and for tundra with standing water (4.4×10^{-3} ; Harper and Wiseman, 1977), which exerts greater drag on wind. Gas concentrations were measured and evasion was estimated on nine dates, during June 20, June 26, July 4, July 9, July 15, July 17, July 26, July 30, and August 3, 2013. Gas concentrations measured at intervals of 0.1 to 0.2 km upstream from Imnavait Weir by the Arctic LTER during June 28 and August 7, 2004 were also analyzed for trends at greater spatial scales.

4.7 Statistics and Error Propagation

Standard measurement errors were propagated following Taylor (1997; Appendix B). All statistical comparisons were made using Single Factor ANOVA and Tukey's Honestly Significant Difference multiple comparisons ($\alpha = 0.05$). Linear regressions ($\alpha = 0.05$) were used to determine whether CO_2 and CH_4 saturation and evasion varied over spatial and temporal scales.

4.0 RESULTS

5.1 Water Balances

Surface inflow to the study reach decreased from 120,000 L h⁻¹ in early July to 24,000 L h⁻¹ in early August, but was consistently 3-4 orders of magnitude greater than subsurface lateral inflows (70 L h⁻¹ to 148 L h⁻¹) throughout the study period (Table 1; Appendix C, Table C1). Evaporation and precipitation were comparatively negligible to water balances. Subsurface lateral inflows typically contributed to less than 0.6 % of total inflow to the study reach. The contribution of subsurface lateral inflows as a percentage of total inflow increased throughout July and early August (Table 1). While this increasing contribution from the subsurface was in part due to decreasing surface inflows, it also resulted from seasonal increases in thaw depth (Figure 3) and thus the expansion of the deeper layer (10 cm depth to the permafrost boundary). For more direct comparisons of subsurface lateral inflows from the shallow (0 to 10 cm depth) and deeper layers, inflows were normalized to per cm of soil depth. Subsurface lateral inflows from the shallow layer (1.1 L h⁻¹ cm⁻¹ ± a standard error, SE, of 0.3 L h⁻¹ cm⁻¹) were significantly greater than subsurface lateral inflows from the deeper layer (Table 2; Appendix C, Table C2) (0.33±SE 0.04 L h⁻¹ cm⁻¹; p<0.001) due to lower hydraulic conductivity from 10 cm depth to the permafrost boundary. Because the deeper layer had a greater volume and lower hydraulic conductivity, water at greater depths also had a significantly longer subsurface residence than did water at shallow depths (p<0.001; Appendix C, Table C3). These residence times ranged from

hours at 0 to 10 cm depth (140 ± 10 min) to days at 10 cm depth to the permafrost boundary (2800 ± 300 min).

Table 1. Summary of water balances by pool and combined as a reach during July 5, July 26, and August 3. Reach-scale terms in the water balances were determined by adding terms for Pools 2 and 3. Subsurface lateral inflows from riparian wetlands on the east and west bank of Innavait Creek at 0 to 10 cm depth and at 10 cm depth to the permafrost boundary are included, in addition to surface inflows and processes (i.e., precipitation and evaporation).

<i>Surface (L/h)</i>	5-Jul			26-Jul			3-Aug		
	<i>POOL 2</i>	<i>POOL 3</i>	<i>REACH</i>	<i>POOL 2</i>	<i>POOL 3</i>	<i>REACH</i>	<i>POOL 2</i>	<i>POOL 3</i>	<i>REACH</i>
Surface Inflow	120000	120032.5		38000	38098.8		24000	24079.3	
Precipitation	0.8	0.7	1.5	0.0	0.0	0.0	0.0	0.0	0.0
Evaporation	0.1	0.1	0.3	0.1	0.1	0.3	0.3	0.3	0.6
Net Surface Inflow	120000.6	120033.2	120071.2	37999.9	38098.7	38147.4	23999.7	24079.0	24136.2
<i>Subsurface (L/h)</i>									
0-10 cm East	4	5	9	22	13	35	17	14.4	31.4
10 cm-Permafrost East	3.7	2.9	6.6	44	23	67	30	25	56
0-10 cm West	13	19	32	11	5	17	11	7.1	17.8
10 cm-Permafrost West	11	11	23	22	7	29	22	10	32
Net Subsurface Inflow	31.9	38.1	70.0	99	49	148	80	57.1	136.8
<i>Percent Total Inflow</i>	0.03	0.03	0.06	0.26	0.13	0.39	0.33	0.24	0.57
<i>Net Outflow</i>	120032.5	120071.2	120071.2	38098.8	38098.7	38295.1	24079.3	24136.2	24136.2

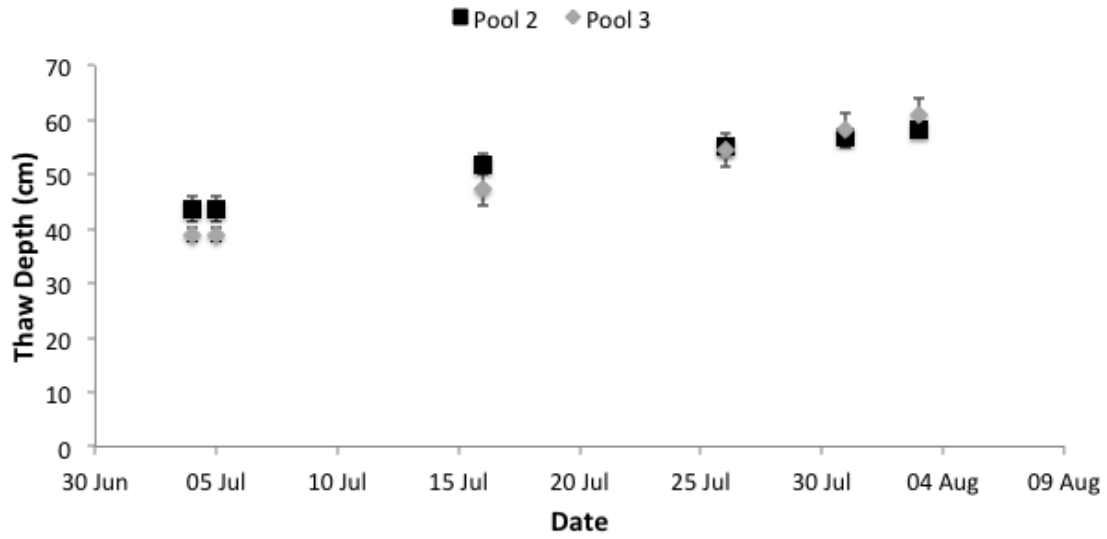


Figure 3. Changing thaw depths near riparian piezometers adjacent to Pools 2 and 3 on the dates of the water balances ($n=24$). Error bars represent the standard error associated with each mean ($n=2$).

Table 2. Subsurface lateral inflows through each cm of the shallow and deeper layers of riparian wetlands on the east and west bank of Imnavait Creek during July 5, July 26, and August 3.

<i>Subsurface (L/h/cm)</i>	5-Jul			26-Jul			3-Aug		
	<i>POOL 2</i>	<i>POOL 3</i>	<i>REACH</i>	<i>POOL 2</i>	<i>POOL 3</i>	<i>REACH</i>	<i>POOL 2</i>	<i>POOL 3</i>	<i>REACH</i>
0-10 cm East	0.4	0.5	0.9	2	1.3	3.5	1.7	1.4	3.1
10 cm-Permafrost East	0.09	0.07	0.16	0.8	0.4	1.2	0.5	0.4	0.9
0-10 cm West	1.3	2	3.2	1	0.5	1.7	1	0.7	1.8
10 cm-Permafrost West	0.3	0.3	0.6	0.4	0.1	0.5	0.4	0.2	0.6

5.2 C Mass Balances

Overall, gas concentrations within subsurface lateral inflows were significantly higher (1-2 orders of magnitude) than within surface inflows ($p < 0.001$). Concentrations of CO_2 within deeper subsurface lateral inflows (10 cm depth to the permafrost boundary) were significantly higher ($18 \pm 1 \text{ mg C L}^{-1}$) than concentrations within shallow subsurface lateral inflows (0 to 10 cm depth) ($11 \pm 1 \text{ mg C L}^{-1}$; $p < 0.001$). Concentrations of CH_4 from the deeper layer ($1.2 \pm 0.1 \text{ mg C L}^{-1}$) were also significantly higher than those from the shallow layer ($0.6 \pm 0.1 \text{ mg C L}^{-1}$; $p < 0.001$). These concentrations did not increase significantly during the study period. There was no significant difference between DOC concentrations within deeper ($2.2 \pm 0.4 \text{ mg L}^{-1}$) and shallow ($2.4 \pm 0.4 \text{ mg L}^{-1}$) subsurface lateral inflows.

Despite concentrations of CO_2 and CH_4 that were much higher within subsurface lateral inflows than within surface inflows, the relatively minor contribution of subsurface water from riparian wetlands to surface waters at Imnavait limited the amount C imported from these wetlands. Of the total CO_2 flowing into Pools 2 and 3, only 0.4-3.7% was from riparian wetlands (Table 3). On average, 97% of the total CO_2 flowing into the study reach was from surface inflows. During July 4 and 5, for example, the study reach received $96,000 \text{ mg CO}_2\text{-C h}^{-1}$ within surface inflow, compared with $990 \text{ mg CO}_2\text{-C h}^{-1}$ within subsurface lateral inflows (Table 3). These proportions were higher for CH_4 ; between 2.3% and 16.3% of $\text{CH}_4\text{-C h}^{-1}$ entering this reach of Imnavait was from riparian wetlands (Table 4). On average, 91% of the total CH_4 flowing into the study reach was from surface inflows. There was no significant difference in the CO_2 or CH_4 imported via subsurface lateral inflows per cm of soil depth from

the shallow or deeper layer, and these per cm imports did not increase significantly during the study period (Appendix D, Tables D1 and D2). As surface inflows decreased and thaw depth increased, the proportions of $\text{CO}_2\text{-C h}^{-1}$ and $\text{CH}_4\text{-C h}^{-1}$ imported by subsurface lateral inflows overall increased (Tables 3 and 4). Like surface water inputs (Table 1), CO_2 within surface inflows decreased from 96,000 during July 4-5 to 42,000 $\text{g CO}_2\text{-C h}^{-1}$ by July 31-August 3 (Table 3). However, CH_4 within surface inflows remained comparatively constant over this period.

Table 3. CO₂ mass balances by pool and combined as a reach during July 4-5, July 26, and July 31-August 3, with standard errors associated with each mean. Reach-scale terms in the C mass balances were determined by adding terms for Pools 2 and 3. CO₂ within subsurface lateral inflows draining riparian wetlands on the east and west bank of Innavait Creek is included (subsurface), both at the shallow and deeper layer. Using the change in mg CO₂-C h⁻¹ per m of stream length, expected mass at Innavait Weir—0.7 km downstream from Pool 3—was calculated.

<i>Surface (mg CO₂-C/h)</i>	4-Jun to 5-Jun			26-Jul			31-Jul-2013 to 3-Aug		
	<i>POOL 2</i>	<i>POOL 3</i>	<i>REACH</i>	<i>POOL 2</i>	<i>POOL 3</i>	<i>REACH</i>	<i>POOL 2</i>	<i>POOL 3</i>	<i>REACH</i>
Surface Inflow	96000	96349±9		58000	59357±20		42000	42720±20	
Surface Evasion	-138±8	-103±8	-237±11	-150±3	-152±2	-301±4	-190±20	-215±20	-740±30
Hyporheic Flux	0.32±0.07	0.33±0.07	0.6±0.1	0.0±0.4	0.0±0.4	0.0±0.6	0.1±0.5	0.1±0.5	0.3±0.7
Water Column Mineralization	1E-04±8E-09	8E-05±6E-09	2E-04±1E-08	1E-04±1E-08	2E-04±1E-08	3E-04±1E-08	1E-04±9E-09	2E-04±2E-08	3E-04±2E-08
Benthic Mineralization	64.10±0.04	64.40±0.04	128.70±0.06	56.39±0.04	64.10±0.04	120.49±0.06	60.00±0.03	60.03±0.03	120.00±0.04
Photomineralization	87.47	62.07	149.54	70.79	66.93	137.72	63.90	63.23	127.13
Mineralization by Hydroxyl Radical	7E-05	1E-04	2E-04	4E-04	6E-04	9E-04	4E-04	7E-04	1E-03
Net Surface Inflow	96018±8	96370±10		57978±3	59340±20		41930±20	42630±30	
<i>Subsurface (mg CO₂-C/h)</i>									
0-10 cm East	18.2±0.1	52±1	71±1	131±3	150±4	281±5	41.8±0.2	80±9	121±9
10 cm-Permafrost East	79.1±0.6	33.77±0.04	113±1	970±20	253±8	1220±20	450±10	189±2	640±10
0-10 cm West	90±1	316±6	406±6	77±1	142±4	219±4	94±6	80±10	170±10
10 cm-Permafrost West	144±3	254±8	398±9	205±1	211±6	416±6	205±3	197±2	402±3
Net Subsurface Inflow	331±4	660±10	990±10	1380±20	760±10	2140±10	790±10	540±10	1330±10
<i>Percent Total Inflow</i>	0.4	0.7	1.0	2.4	1.3	3.7	1.9	1.3	3.2
<i>Expected Net Outflow</i>	96349.41	97028.88	97028.88	59357.42	60092.26	60092.26	42720.95	43170.95	43171
<i>Measured Net Outflow</i>			100000			66000			47000
<i>Change in Mass per h</i>			4000			8000			5000
<i>Change in Mass per h per m Stream Length</i>			276			552			345
<i>Imported:Exported</i>			0.96			0.88			0.89
<i>Expected Weir Inflow</i>			285306			436612			278632
<i>Observed Weir Inflow</i>			158800±400			87000±1000			17800±300

Table 4. CH₄ mass balances by pool and combined as a reach during July 4-5, July 26, and July 31-August 3, with standard errors associated with each mean. Reach-scale terms in the C mass balances were determined by adding terms for Pools 2 and 3. CH₄ within subsurface lateral inflows draining riparian wetlands on the east and west bank of Innavait Creek is included (subsurface), both at the shallow and deeper layer. Using the change in mg CH₄-C h⁻¹ per m of stream length, expected mass at Innavait Weir—0.7 km downstream from Pool 3—was calculated.

<i>Surface (mg CH₄-C/h)</i>	4-Jul to 5-Jul			26-Jul			31-Jul to 3-Aug		
	<i>POOL 2</i>	<i>POOL 3</i>	<i>REACH</i>	<i>POOL 2</i>	<i>POOL 3</i>	<i>REACH</i>	<i>POOL 2</i>	<i>POOL 3</i>	<i>REACH</i>
Surface Inflow	900	919.3±0.4		780	852±1		900	946±3	
Surface Evasion	-1.4±0.1	-1.0±0.1	-2.4±0.2	-2.2±0.1	-3.01±0.02	-5.2±0.1	-4.7±0.1	-0.8±0.1	-5.5±0.2
Hyporheic Flux	0.05±0.01	0.034±0.008	0.08±0.01	0.00±0.04	0.00±0.04	0.00±0.06	0.00±0.03	0.00±0.03	0.00±0.04
Net Surface Inflow	898.6±0.1	897.67±0.09		777.8±0.1	774.77±0.05		895.3±0.1	894.5±0.1	894.5±0.2
<i>Subsurface (mg CH₄-C/h)</i>									
0-10 cm East	0.9±0.1	5.2±0.3	6.1±0.4	4.8±0.2	9.6±0.3	14.4±0.4	0.4±0.3	3.2±0.5	4±1
10 cm-Permafrost East	6.1±0.1	3.8±0.1	9.9±0.1	59±1	26±1	84±1	28±1	17±1	45±1
0-10 cm West	0.07±0.02	20.3±0.7	21±1	1.3±0.1	7.3±0.1	8.6±0.1	6.8±0.4	4.6±0.5	11±1
10 cm-Permafrost West	13.0±0.3	12±1	25±1	9.9±0.1	9.4±0.1	19.3±0.2	15±3	10.9±0.1	26±3
Net Subsurface Inflow	20.7±0.4	41±1	62±2	75±1	52±1	127±2	51±3	35±1	86±3
<i>Percent Total Inflow</i>	2.3	4.6	6.9	9.6	6.7	16.3	5.7	4.0	9.6
<i>Expected Net Outflow</i>	919.31	959.54	959.54	852.37	901.41	901	946.02	980.56	980.56
<i>Measured Net Outflow</i>			900			1200			1300
<i>Change in Mass per h</i>			0			420			400
<i>Change in Mass per h per m Stream Length</i>			0			29			28
<i>Imported:Exported</i>			1.00			0.65			0.69
<i>Expected Weir Inflow</i>			900			20657			19831
<i>Observed Weir Inflow</i>			2310±40			1950±50			420±30

Import and export of DOC varied between July 26 and July 31-August 3. Like CO₂ and CH₄, most DOC was imported by surface inflow during July 26. Unlike CO₂ and CH₄, >1000 mg DOC h⁻¹ was consumed along the study reach on this date, most of it from surface inflow (Appendix D, Table D3). DOC measured within subsurface lateral inflows accounted for a negligible fraction of total DOC inflow during July 26, but this fraction increased to nearly 25% during July 31-August 3 (Appendix D, Table D3). However, fewer samples were collected on fewer dates for DOC, making these estimates more subject to error.

Terms that contributed to the CO₂ mass balance on orders of magnitude similar to subsurface lateral inflows included benthic respiration, photo-mineralization, and evasion (Table 3). Between 14% and 30% of CO₂-C h⁻¹ entering the study reach within subsurface lateral inflows was immediately lost to the atmosphere via surface evasion (Table 3). This proportion decreased from July 4 (25%) and July 26 (14%), but increased again on August 3 (30%) with the development of thermal stratification (section 5.5, Figure 6). A much smaller proportion of CH₄ imported to the study reach within subsurface lateral inflows was lost to the atmosphere (between 4% and 6%), despite its lower solubility in water than CO₂. These proportions also increased from July 4 (4%) to August 3 (6%).

Hyporheic flux (Appendix D, Figures D1 and D2), in-stream respiration (Appendix E), and abiotic oxidation of OM by •OH were comparatively negligible terms in the C mass balances (Tables 3 and 4). The effect of stratification on mg CO₂-C h⁻¹ in surface outflow was also tested by dividing the pools into an upper volume of water influenced only by surface inflow and a lower volume of water influenced only by subsurface lateral inflows (section 5.5). Although this

test increased the export of $\text{mg CO}_2\text{-C h}^{-1}$ produced by water column respiration from 0.0003 ± 0.0001 mg to 0.0034 ± 0.0005 $\text{mg CO}_2\text{-C h}^{-1}$ and the mineralization by $\bullet\text{OH}$ from 0.0007 ± 0.0003 to 0.10 ± 0.02 $\text{mg CO}_2\text{-C h}^{-1}$ at the reach scale, these terms remained negligible to the CO_2 mass balances.

5.3 Chemical Structure of DOM

Although DOC and TDN concentrations were significantly higher within shallow and deeper subsurface lateral inflows than within surface inflows ($p=0.04$), molar DOC:TDN was fairly uniform within both surface and subsurface lateral inflows (34 ± 3 ; Table 5). This was also true for S_R values, which consistently indicated the presence of more high than low molecular weight CDOM within both surface and subsurface lateral inflows (Table 5; Helms et al., 2008). These S_R values did not vary significantly from the surface to the subsurface, though a_{300} values indicated significantly more CDOM at 0 to 10 cm depth ($p=0.05$) and at 10 cm depth to the permafrost boundary ($p=0.04$) than in surface inflows (Table 5; Cory et al., 2013). There were significant differences in another measure of DOM quality: the aromaticity or amount of humus present within CDOM. Soil humus, subdivided into humic acids, fulvic acids, and humin, is aromatic (Weishaar et al., 2003). Aromatic compounds are characterized by stable, conjugated rings of unsaturated bonds (Schwarzenbach et al., 2003). The stability of these structures, which are usually of high molecular weight (e.g., high S_R), makes them relatively recalcitrant to microbial mineralization. Fulvic acid aromaticity estimated by FI was significantly greater at deeper subsurface depths than at shallow depths ($p=0.03$). Fulvic acid aromaticity at shallow subsurface depths was significantly greater than in surface waters (Table 5; $p=0.002$). Despite

C:N ratios that imply uniform lability of DOM imported to the study reach by surface and subsurface waters, the aromaticity of CDOM was greater within subsurface lateral inflows, and greatest within subsurface lateral inflows from the deeper layer. This suggests that DOM lability decreases with soil depth.

Table 5. Indices of DOM quality measured within Imnavait Creek ($n=8$ samples) and subsurface lateral inflows at 0 to 10 cm depth ($n=8$) and at 10 cm depth to the permafrost boundary ($n=8$). The C:N molar ratio, Total Dissolved N and DOC concentrations, slope ratio (S_R), CDOM content of DOM (a_{300}), total humic content ($SUVA_{254}$), and fulvic acid aromaticity (FI) are included, with standard errors associated with each mean.

	In stream	0 to 10 cm Depth	10 cm Depth to the Permafrost Boundary
C:N (molar)	34±2	34±3	34±3
TDN (mg/L)	0.48±0.02	0.70±0.07	0.6±0.1
DOC (mg/L)	14.2±0.2	21±2	21±2
S_R	0.77±0.01	0.74±0.07	0.77±0.9
a_{300} (m^{-1})	64±7	140±80	140±60
$SUVA_{254}$	3.7±0.3	5±1	5±1
FI	1.56±0.02	1.61±0.02	1.66±0.03

5.4 Wetland Processing

Similar to subsurface sampling carried out near piezometers for the C mass balances, subsurface sampling carried out at riparian transect points showed one to two orders of magnitude more dissolved CO₂ and CH₄ in soil waters than in adjacent surface waters (Appendix E, Figures E1 and E2). Concentrations of dissolved CO₂ were significantly higher at riparian transect points without standing water at the surface (“dry”) than at those with standing water at the surface (“wet”) in late June (p=0.001), early July (p=0.003), and early August (p=0.02). Concentrations of dissolved CH₄ were significantly higher at dry riparian transect points than at wet transect points in late June (p=0.05), only. Furthermore, transect point concentrations of both CO₂ and CH₄ were significantly higher at 10 cm depth to the permafrost boundary than at 0 to 10 cm depth in early July (p<0.001 for CO₂ and CH₄) and early August (p=0.05 for CO₂, p<0.001 for CH₄), though concentrations in the deeper layer were not measured in late June (Appendix E, Tables E3 and E4). There was no significant difference between concentrations of these dissolved gases sampled 1 m and 6 m from the pool edge (Appendix E, Tables E1-E4). For CO₂, transect point concentrations were significantly higher in July (18±4 mg C L⁻¹) and August (18±2 mg C L⁻¹) than in June (9.8±0.9 mg C L⁻¹; p<0.001). A similar trend was observed for CH₄; transect point concentrations of CH₄ were significantly higher during August 3 (0.95±0.09 mg C L⁻¹) than during June 26 (0.46±0.07 mg C L⁻¹; p<0.001). Thus, the deeper layers of Innavait’s riparian wetlands without standing water contributed most CO₂ and CH₄ to subsurface lateral inflows, and this contribution increased throughout the summer study period.

Based on incubations of riparian wetland soil cores, CO₂ was produced at rates ranging from 0.7 to 4.9 μmol CO₂ L⁻¹ h⁻¹ g⁻¹ (Appendix E, Table E5). CO₂ production was significantly greater at 6 m from the pool edge (3.3±0.4 μmol CO₂ L⁻¹ h⁻¹ g⁻¹) than at 1 m (2.0±0.1 μmol CO₂ L⁻¹ h⁻¹ g⁻¹, p=0.004; Appendix E, Table E5). While CO₂ production tended to be higher in the shallow layer (4.8±0.7 μmol CO₂ L⁻¹ h⁻¹ g⁻¹) than in the deeper layer (3±1 μmol CO₂ L⁻¹ h⁻¹ g⁻¹), these differences were not statistically significant (Appendix E, Table E5). CO₂ production was consistently 1-2 orders of magnitude higher in soil and sediment cores than in surface and soil waters from the pools of Imnavait Creek (Figure 4; p<0.001). However, soil cores collected from the hill slope produced significantly less CO₂ than cores collected from riparian wetlands (p=0.006) and pool sediments (p=0.005), emphasizing the importance of riparian wetlands and the pool bottom to local biogeochemical cycling (Figure 4). Among the different hill slope soils sampled, CO₂ production was significantly greater within a water track (1.7±0.4 μmol CO₂ L⁻¹ h⁻¹ g⁻¹) and the shallow organic layer of hill slope soils outside of this water track (1.1±0.2 μmol CO₂ L⁻¹ h⁻¹ g⁻¹) than in the deeper mineral layer (0.33±0.04 μmol CO₂ L⁻¹ h⁻¹ g⁻¹, p=0.006; Appendix F, Table F5). All soils and sediments can be classified as peat, with the exception of this deeper mineral layer. These results represent aerobic microbial mineralization over a shallow volume of soils and sediments. It is probable that microbial mineralization occurs via anaerobic pathways at greater subsurface depths than cores were collected. Therefore, results represent a minimum estimate for CO₂ production in these environments, but show that the greatest consumption of O₂ and production of CO₂ at Imnavait is in riparian and pool bottom peat.

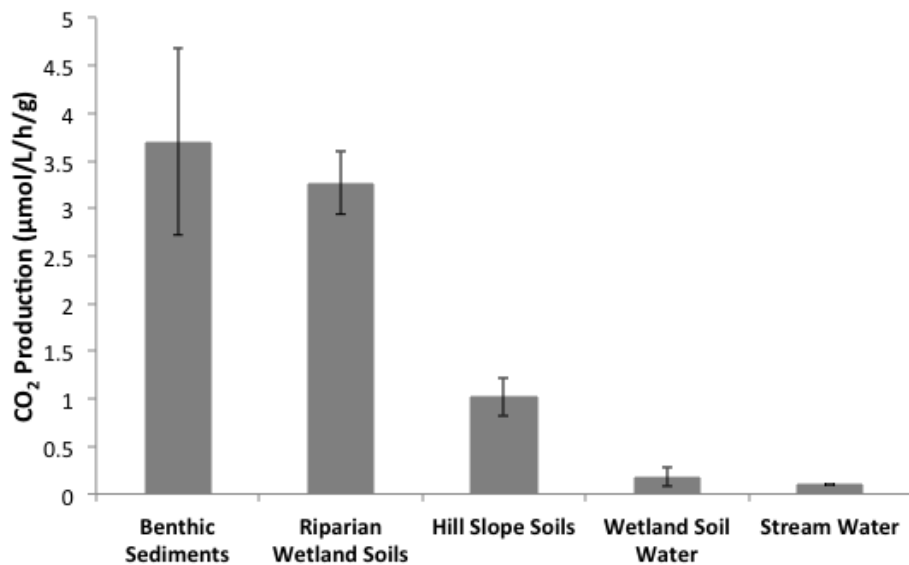
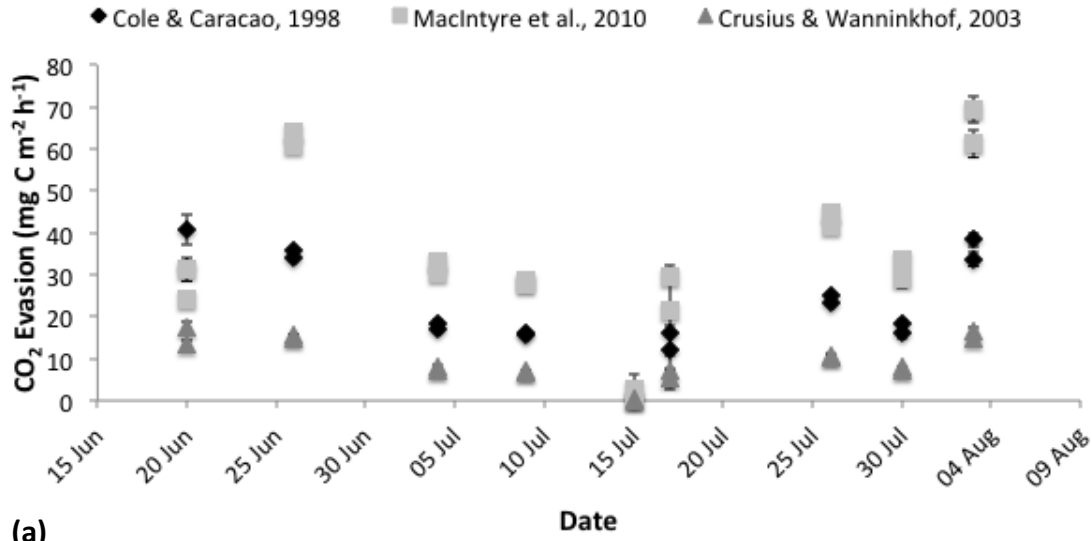


Figure 4. CO₂ produced in wetland soil cores ($n=39$), wetland soil water ($n=9$), hill slope soil cores ($n=18$), pool sediment cores ($n=17$), and pool water ($n=24$), in $\mu\text{m L}^{-1} \text{h}^{-1}$ of incubation time. Error bars represent the standard error associated with each mean ($n=3$). All soils and sediments can be classified as peat; no mineral soils from the deeper layer are included. CO₂ production was normalized to the dry weight (g) of soil and sediment cores where applicable.

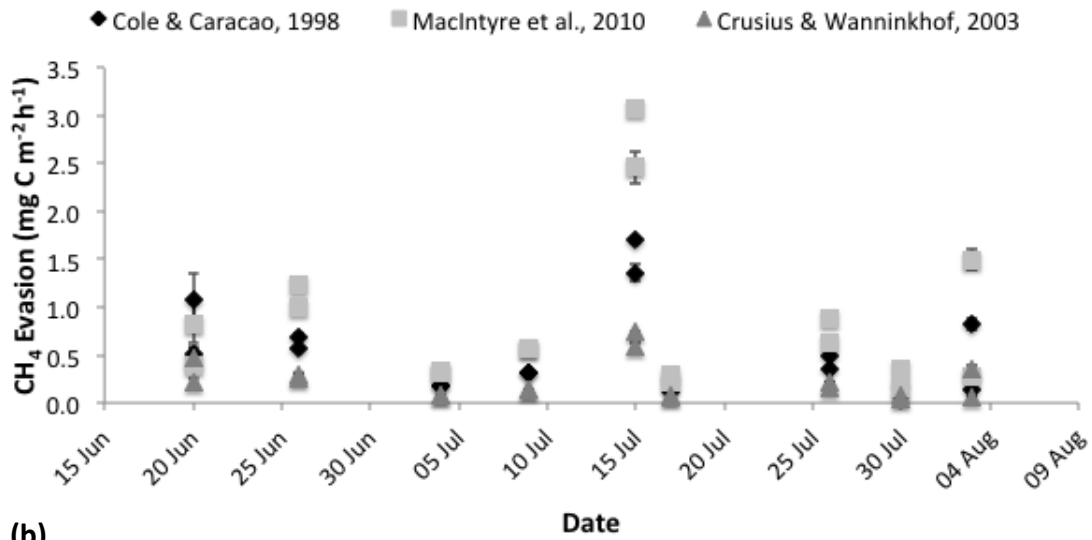
5.5 *In-stream Gas Concentrations and Evasion*

The mean partial pressure of CO₂ was 3000±300 µatm in both Pools 2 and 3 during the June 20 to August 6 study period ($n=51$). Mean CH₄ was 1400±200 in Pool 2 ($n=26$) and 1300±SE 200 µatm in Pool 3 ($n=25$) during this period. Calculated partial pressures in equilibrium with the atmosphere were 348±4 µatm CO₂ and 2.1±0.1 µatm CH₄. Thus, surface waters in Pools 2 and 3 of Innavait Creek were supersaturated with respect to atmospheric CO₂ and CH₄, leading to the evasion of these gases to the atmosphere.

CO₂ evasion rates estimated using MacIntyre et al. (2010)'s k_{600} relationships were significantly greater than evasion rates estimated following Cole and Caracao (1998) ($p=0.01$), which were significantly greater than evasion rates estimated following Crusius and Wanninkhof (2003; Figure 5a) ($p=0.02$). CH₄ evasion rates estimated using MacIntyre et al. (2010)'s k_{600} relationships were significantly greater than evasion rates estimated following Crusius and Wanninkhof (2003; Figure 5b) ($p=0.004$). Water along the study reach was warmer than the atmosphere (except during June 20). Therefore, these results imply that convective cooling at the water's surface may increase gas evasion. Because the thin boundary-layer equation generally provides a minimum estimate of gas evasion when compared to other methods (Schubert et al., 2012), and because evasion rates estimated following Cole and Caracao (1998) represent a middle range, we report evasion rates estimated following Cole and Caracao (1998) hereafter. We used a drag coefficient estimated for tundra with standing water, although there was no significant difference between evasion rates estimated using a frictionless drag coefficient.



(a)

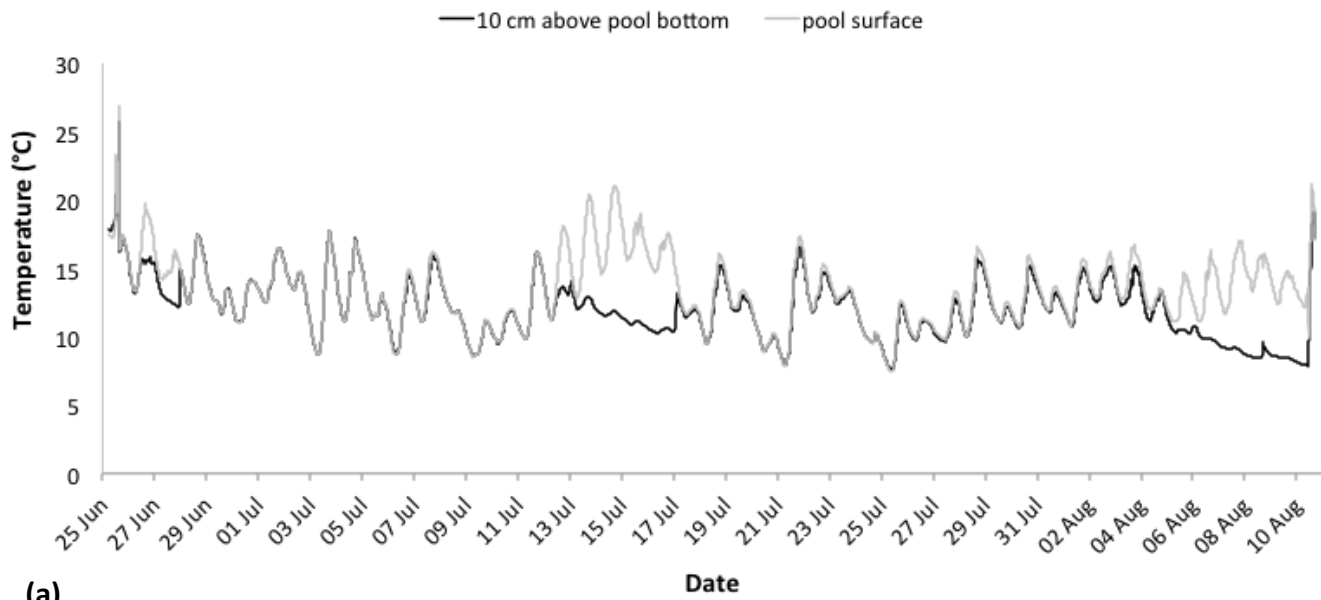


(b)

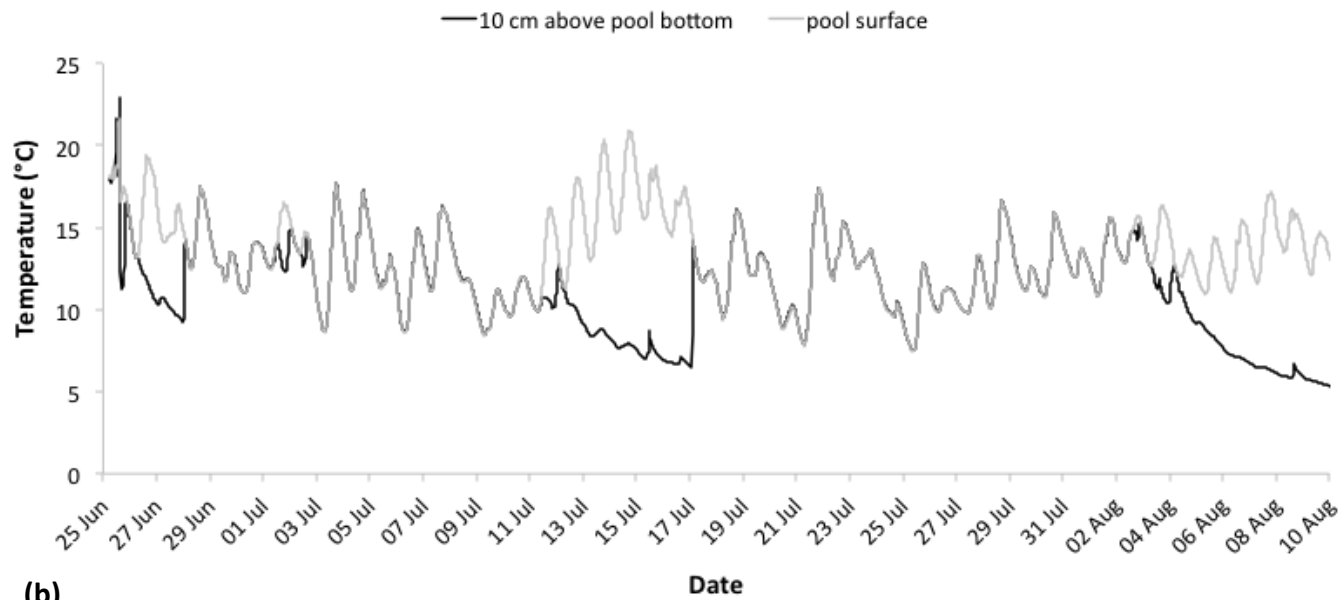
Figure 5. Evasion rates for CO₂ (a) and CH₄ (b) estimated using k_{600} relationships published by Cole and Caracao (1998), MacIntyre et al. (2010), and Crusius and Wanninkhof (2003). Error bars represent the standard error associated with each mean ($n=2$).

Overall, in-stream gas concentrations ($n=51$) and evasion rates ($n=51$) of CO_2 ($22\pm 2 \text{ mg C m}^{-2} \text{ h}^{-1}$) and CH_4 ($0.53\pm 0.07 \text{ mg C m}^{-2} \text{ h}^{-1}$) did not vary significantly from Pool 2 to Pool 3. However, thermal stratification developed in the pools during June 20¹, June 26, July 15, and August 3 (Figure 6). During stratification, CO_2 was significantly greater in surface waters along the study reach ($4400\pm 200 \text{ } \mu\text{atm}$) than when the pools were well mixed ($2080\pm 90 \text{ } \mu\text{atm}$; $p<0.001$). Surface water CO_2 also became more variable during stratification between Pool 2 ($4200\pm 400 \text{ } \mu\text{atm}$) and Pool 3 ($4600\pm 300 \text{ } \mu\text{atm}$). Stratification had the same effect on CH_4 in surface waters ($2200\pm 300 \text{ } \mu\text{atm}$) relative to mixed conditions ($650\pm 70 \text{ } \mu\text{atm}$; $p=0.02$), and CH_4 was also more variable from Pool 2 ($2400\pm 400 \text{ } \mu\text{atm}$) compared to Pool 3 ($2100\pm 400 \text{ } \mu\text{atm}$) during stratification. Higher gas concentrations in surface waters during stratification led to higher evasion rates. Evasion of CO_2 was significantly higher along the study reach during stratification ($28\pm 4 \text{ mg C m}^{-2} \text{ h}^{-1}$) than when waters were well mixed ($16.8\pm 0.8 \text{ mg C m}^{-2} \text{ h}^{-1}$; $p<0.001$), and was also more variable between Pool 2 ($25\pm 5 \text{ mg C m}^{-2} \text{ h}^{-1}$) and Pool 3 ($30\pm 2 \text{ mg C m}^{-2} \text{ h}^{-1}$). The same was true for CH_4 evasion rates ($0.9\pm 0.1 \text{ mg C m}^{-2} \text{ h}^{-1}$) relative to mixed conditions ($0.23\pm 0.02 \text{ mg C m}^{-2} \text{ h}^{-1}$; $p<0.001$), which were also more variable between Pool 2 ($0.9\pm 0.2 \text{ mg C m}^{-2} \text{ h}^{-1}$) and Pool 3 (Figure 7) ($0.89\pm 0.05 \text{ mg C m}^{-2} \text{ h}^{-1}$).

¹ Stratification is assumed to have developed in Imnavait pools on June 20 based on increases in CO_2 and CH_4 in bottom waters, although thermistor chains were not deployed until June 25.

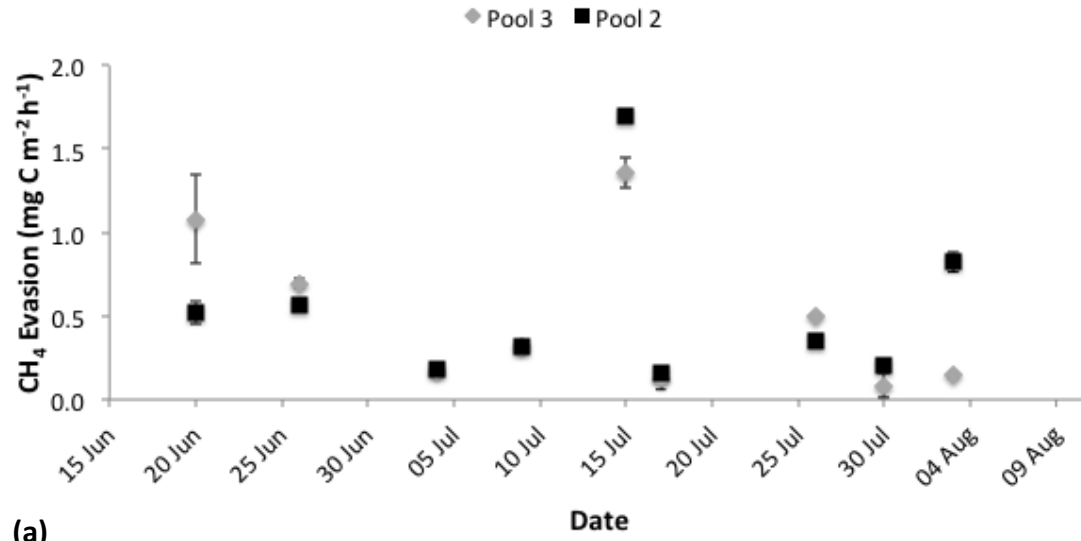


(a)

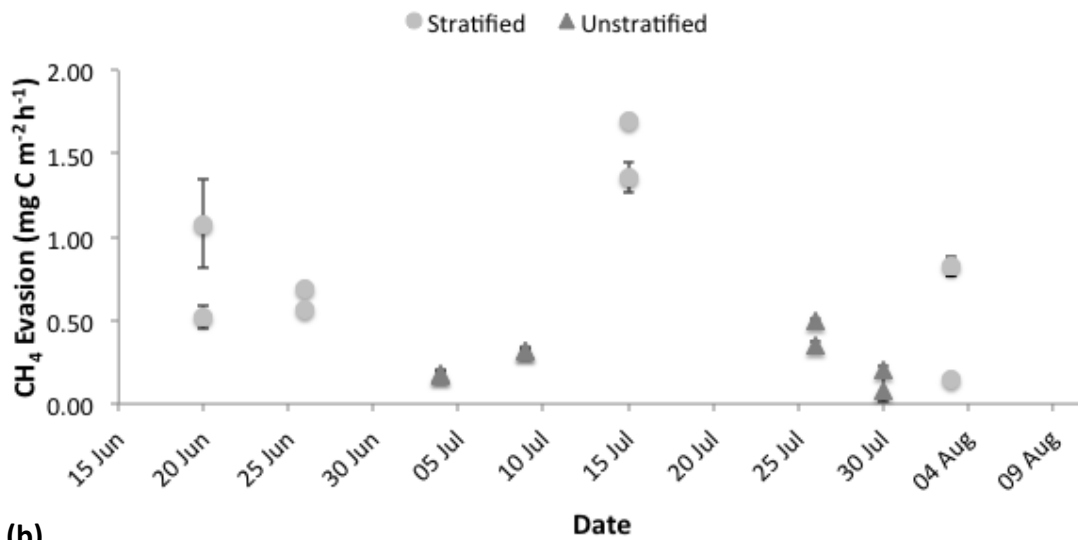


(b)

Figure 6. Stratification that developed in Pool 2 (a) and Pool 3 (b) of Innvait Creek recorded by thermistors 10 cm above the pool bottom and at the pool surface.



(a)



(b)

Figure 7. CH₄ evasion rates (mg C m⁻² h⁻¹) from Pools 2 and 3 during the study period (a) ($n=51$). Error bars represent the standard error associated with each mean ($n=3$). CH₄ is significantly greater during stratification in Pools 2 and 3 (b) ($p<0.001$). The same trends were observed for CO₂ evasion and for CO₂ and CH₄ partial pressures.

CO₂ (1900±100 μatm) was significantly lower 0.7 km downstream, at Imnavait Weir, than in Pools 2 and 3 (p=0.02). This is consistent with measurements of CO₂ showing a significant positive correlation between CO₂ (Figure 8a; Arctic LTER) ($\square^2=0.36$, p=0.01, *df*=14) and distance upstream from the reference site at Imnavait Weir during June 2004. This spatial trend weakened by August 2004 (Figure 8b) ($\square^2=0.18$, p=0.04, *df*=8). Similarly, CH₄ in this data set increased significantly with distance upstream in June 2004 ($\square^2=0.49$, p=0.002, *df*=14), though not in August (Appendix F, Figure F1). In contrast, CH₄ was significantly higher at Imnavait Weir (780±10 μatm, p<0.001) than in Pools 2 and 3 during the 2013 study period. Furthermore, CH₄ at this downstream site increased significantly from June 19 (600±200 μatm) to August 6, 2013 (Figure 9) (1600±100 μatm; $r^2=0.35$, p=0.04, *df*=11). CO₂ partial pressures remained comparatively constant at Imnavait Weir from June 19 to August 6, 2013 (Appendix F, Figure F2) (1900±100 μatm). Evasion was not estimated at Imnavait Weir and compared to the study reach because Imnavait Weir lacks pools, and therefore a comparable surface area and diffusion conditions.

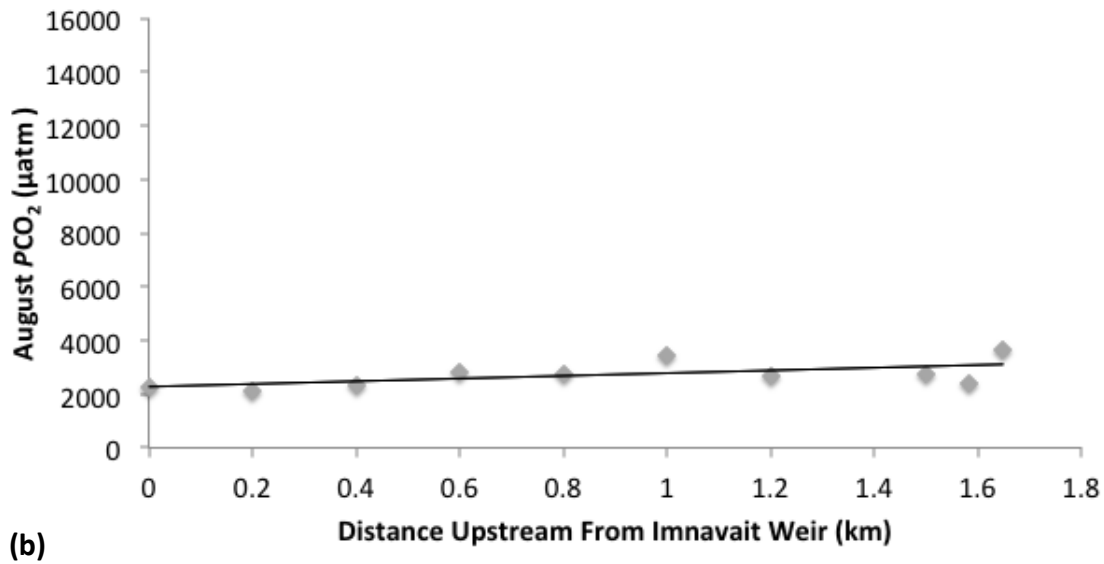
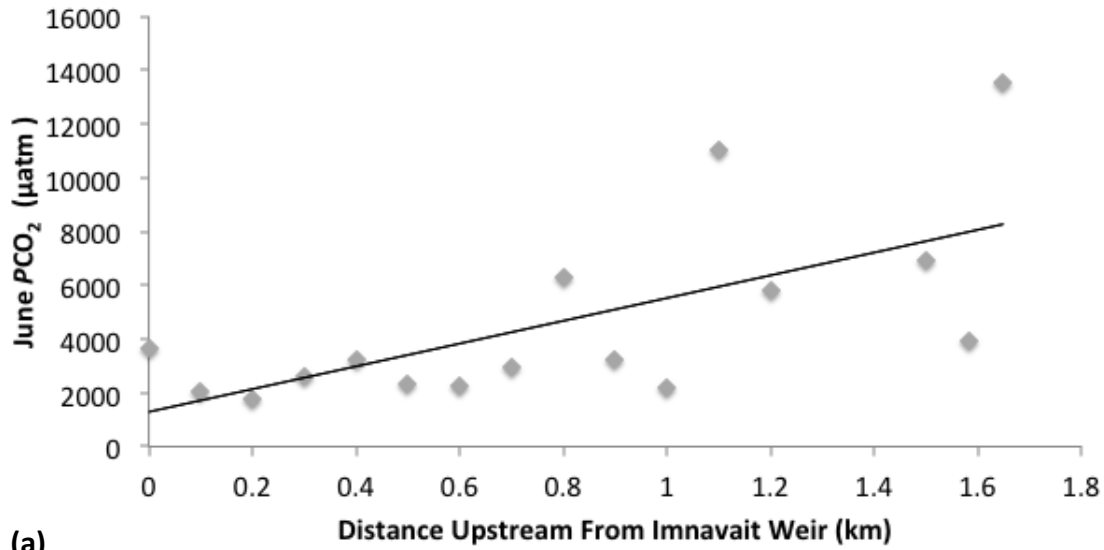


Figure 8. CO₂ (µatm) from Imnavait Weir (0 km) to 1.7 km upstream measured by the Arctic LTER on June 28 (a) and August 8 (b), 2004. Similar trends were observed for CH₄ on June 28, 2004.

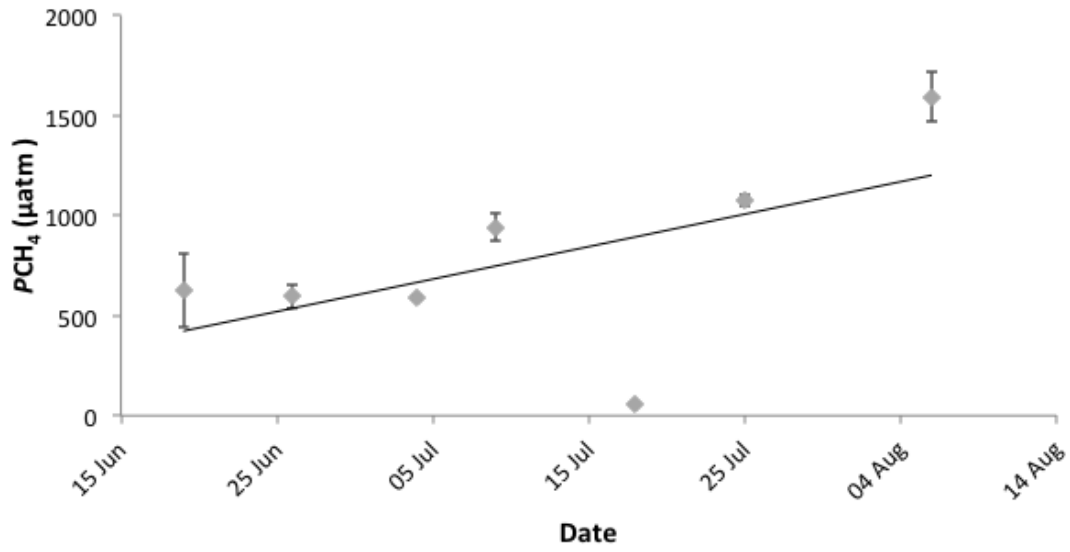


Figure 9. CH₄ (µatm) at Imnavait Weir from June 20 to August 6, 2013 ($n=14$). Error bars represent the standard error associated with each mean ($n=2$).

5.0 DISCUSSION

Terrestrial-aquatic C transfers within subsurface lateral inflows from riparian wetlands were a small fraction of the total CO₂ and CH₄ moving through our study reach in surface inflows (Tables 2 and 3). Despite concentrations of these constituents that were 1-2 orders of magnitude higher in subsurface soil waters than in stream waters, terrestrial-aquatic transfers along a short stream reach (meters) were limited because subsurface lateral inflows generally accounted for >0.1% of inflow into the reach (Table 1). However, subsurface C inputs along a reach are integrated moving up or downstream, and over a sufficient distance these subsurface lateral inflows can account for the mass of C carried in surface waters. Using measured values and the length of the study reach (14.5 m), subsurface lateral inflows contributed 276 to 552 mg CO₂-C h⁻¹, 0 to 29 mg CH₄-C h⁻¹, and up to 69 mg DOC h⁻¹ to each m of Innavait Creek. Multiplying these values by the distance from our study reach to the upstream source of Innavait, subsurface lateral inputs are more than enough to explain the mass flux of C observed within surface water. If similar subsurface lateral inflows are assumed from the study reach to the headwater stream source, then between 120 and 363 m of stream length are required to produce the C flux of CO₂ observed entering the study reach in surface water. These lengths are between 41 and 47 m for CH₄ and 36 m for DOC. Because the distance from the upstream source of Innavait Creek to the outflow of Pool 3 is approximately 428 m, there must be a loss of CO₂, CH₄, and DOC along the stream to account for the lower fluxes than predicted of materials entering the study reach. This loss was likely due to photochemical and biological mineralization of DOC, and to gas evasion because other loss terms in the C mass balances were comparatively negligible.

Surface water concentrations of CO₂ and CH₄ were generally higher in this arctic headwater stream than in adjacent lakes and rivers, as well as in boreal and temperate headwater streams (Table 5). CH₄ concentrations were significantly higher downstream, at Innavait Weir, than upstream, at the study reach. This may result from little of the CH₄ within subsurface lateral inflows (4-6%) evading from surface waters to the atmosphere along the study reach (Table 3). However, CO₂ concentrations decreased significantly from the study reach to Innavait Weir, which is consistent with prior measurements in June and July, 2004 (Figure 8). Furthermore, the evasion of C from CO₂ along the study reach was greater than from CH₄ (Tables 2 and 3). The same decrease in CO₂ partial pressures documented by this study from upstream to downstream in a single arctic headwater stream has been documented by boreal and temperate studies at the river network scale, from headwater streams to rivers (Jonsson et al., 2007; Teodoru et al., 2009; Humborg et al., 2010; Crawford et al., 2013). As streams become narrower and shallower upstream, the surface area of water in contact with land increases. Thus, the influence of terrestrial-aquatic C transfers on surface water chemistry increases further upstream from Innavait Weir, or the further upstream from a river to a headwater stream. At Innavait, we consistently observed gas concentrations in subsurface soil waters that were much higher than gas concentrations in stream waters, and present the first direct measurements of terrestrial-aquatic transfers of C within subsurface lateral inflows of soil water from riparian wetlands to an arctic headwater stream.

Table 5. Partial pressures (μatm) of CO_2 and CH_4 observed at Imnavait and elsewhere on the North Slope. Though not a comprehensive list, other studies of headwater streams at lower latitudes are included for comparison.

Site	Study	Year	PCO_2 (μatm)	PCH_4 (μatm)
<i>Arctic, Alaska North Slope</i>				
Headwater stream, stratified pool	<i>This study</i>	2013	4400 \pm 200	2200 \pm 300
Headwater stream, mixed pool	<i>This study</i>	2013	2080 \pm 90	650 \pm 70
Headwater stream, downstream ref.	<i>This study</i>	2013	1900 \pm 99	780 \pm 13
Toolik Lake inlet	<i>Arctic LTER</i>	2013	961	56
Toolik Lake outlet	<i>Arctic LTER</i>	2013	448	25
Lake NE14	<i>Arctic LTER</i>	2013	950	85
Kuparuk River	<i>Arctic LTER</i>	2012	4000 \pm 2000	24 \pm 10
<i>Boreal</i>				
Small streams	<i>Aufdenkampe et al.</i>	2011	1300	
Small streams, Alaska	<i>Crawford et al.</i>	2013	570-2600	4
Headwater streams, Sweden	<i>Humborg et al.</i>	2010	1445	
Small streams, Canada	<i>Teodoru et al.</i>	2009	2243	
<i>Temperate</i>				
Headwater streams, U.S.	<i>Butman and Raymond et al.</i>	2011	3120	
Headwater streams, U.S.	<i>Hope et al.</i>	2004	424-2674	142-879
Headwater streams, U.S.	<i>Jones and Mulholland</i>	1998	3340	306

Gas concentrations and evasion increased significantly during periods of thermal stratification compared to periods when the pools were well mixed (Figure 7b). During stratification, the chemistry of the bottom waters is more likely influenced by inputs from subsurface soil waters than by surface waters (Merck et al., 2012), receiving significantly higher concentrations of CO₂ and CH₄ within subsurface lateral inflows (Tables 2 and 3). This CO₂ and CH₄ likely accumulates in bottom waters due to longer water residence times (Merck et al., 2012). As higher velocity surface inflows (Table 1) move across the thermocline and the more stagnant waters of the bottom, resulting advection may cause eddies of CO₂- and CH₄-rich water from the bottom to rise to the surface. Here, higher partial pressures of CO₂—some of which may be oxidized CH₄—and CH₄ from bottom waters contribute to higher evasion rates. During stratification, evasion of both CO₂ and CH₄ were significantly elevated above mixed conditions. Assuming a mean pool surface area of 6 m², we estimate that stratification led to the evasion of an additional 4000±600 mg CO₂-C and 130±14 mg CH₄-C along the study reach from June 20 to August 6, 2013. It is generally thought that lake mixing increases CO₂ and CH₄ in surface waters by bringing nutrients, DOM in senesced phyto- and zooplankton (Kirillin et al., 2012), etc., CO₂, and CH₄ from the bottom to the surface, where more efficient oxidation and evasion may occur. Mixing has been shown to increase CO₂ evasion nearby, in Toolik Lake (Eugster et al., 2003). Contrary to the sequestration of DOM and dissolved gases in bottom waters during stratification, these findings at Imnavait could therefore have implications for other stratified systems with high surface water velocity and strong terrestrial-aquatic linkages through the subsurface.

Photo-mineralization of DOC to CO₂ was another important term in the C mass balances (Table 2). On July 26, for example, 1,000 mg of DOC h⁻¹ was lost from Pool 2 to Pool 3 along the study reach (Appendix D, Table D1). Water column mineralization by microbes was comparatively low, perhaps

due to the high aromatic content of DOM entering the length of Imnavait within subsurface lateral inflows (a_{300} ; Table 5). The most labile DOM within subsurface soil waters was likely consumed before it reached Imnavait in riparian wetlands (Judd and Kling, 2002), indicated by the high microbial mineralization rates in these soils (Figure 4). While highly aromatic DOM compounds are more resistant to microbial oxidation than other, aliphatic DOM compounds, these aromatics are also more susceptible to photo-degradation (Ward et al., 2014). Differences in aromaticity between surface and subsurface flow paths suggest either that subsurface lateral inflows contain inherently more aromatic DOM than surface inflows, or that aromatic DOM is transformed by abiotic in-stream processes, such as photo-degradation (Cory et al., 2013) or incomplete oxidation by $\bullet\text{OH}$ (Page et al., 2013). In this study, mineralization by $\bullet\text{OH}$ was comparatively unimportant to the C mass balances (Table 2). Therefore, sunlight is responsible for most mineralization of DOC to CO_2 .

In the riparian wetlands last encountered by subsurface lateral inflows before Imnavait Creek, concentrations of CO_2 and CH_4 were significantly higher at 10 cm depth to the permafrost boundary than at 0 to 10 cm depth. At this deeper layer, residence time was also greater due to lower hydraulic conductivity and greater subsurface volume, indicating that water interacted with peat over a greater surface area for longer periods ($2800 \pm \text{SE } 300$ min at 10 cm depth to the permafrost boundary, compared to $140 \pm \text{SE } 10$ min at 0 to 10 cm; Appendix C, Table C3), which allowed for more CO_2 and CH_4 to dissolve (Mulholland, 1993). A seasonal increase in thaw depth (Figure 3) is one factor that led to an increase in terrestrial-aquatic transfers from the deeper layer during the summer study period (Tables 2 and 3). These findings have implications for scenarios of climate change. Temperature changes have been most acute thus far in high latitudes, increasing $0.6 \text{ }^\circ\text{C y}^{-1}$ above 62°N , compared to $0.35 \text{ }^\circ\text{C y}^{-1}$ between 50° and 70°N , since 1985 (Serreze and Francis, 2006; Euskirchen et al., 2007). In the southern

reaches of the Kuparuk River Basin, where Innavait Creek is located, the magnitude of annual temperature increases as predicted by five Global Circulation Models is much lower (~ 0.04 °C y^{-1} through 2099), though with warmer winters and strong interannual variability (Cherry et al., 2014). Rising temperatures may cause thermal erosion of permafrost (Polyakov et al., 2002). This will increase not only the amount of OM available to microbial oxidation, highest in wetland soils and pool sediments (Figure 4), but also the volume of the deeper layer. In other words, the expansion of the active layer from 10 cm depth to the permafrost boundary, and associated increases in terrestrial-aquatic CO₂ and CH₄ transfers that we observed over July, may demonstrate that greater C exports from wet sedge tundra are likely during some years under scenarios of climate change. Another prediction of these models is a two-fold increase in summer precipitation (Cherry et al., 2014). Greater precipitation in the Innavait catchment will likely lead to a decrease in insolation and an increase in discharge, potentially making thermal stratification in Innavait pools and its effects on gas evasion rarer.

6.0 CONCLUSIONS

Our results indicate that terrestrial-aquatic C transfers from riparian wetlands along the length of Innavait Creek lead to the supersaturation of this arctic headwater stream with CO₂ and CH₄ relative to atmospheric levels. This supersaturation increases during periods of thermal stratification in the stream pools, and results in the evasion of greenhouse gases to the atmosphere. Evasion of up to 1/3 of the CO₂ introduced to Innavait within subsurface lateral inflows and decreasing concentrations of CO₂ from upstream to downstream are consistent with studies of boreal and temperate headwater streams. Collectively, these studies show that headwater streams not only connect a large terrestrial organic C

pool to other conduits for CO₂ to the atmosphere, such as larger rivers, but themselves serve as an important conduit. Prior to this study, little data had been collected on terrestrial-aquatic transfers of CH₄ and its subsequent transport or evasion from headwater streams. We show that much less C from CH₄ evades as water moves from upstream to downstream than does C from CO₂ at Imnavait. Perhaps because of these lower evasion rates, CH₄ increases in stream waters from upstream to downstream. In addition to evasion, photo-mineralization is an important term in the C mass balances for this arctic headwater stream during its ice-free season, when insolation incidentally occurs for the majority of each day. While global change may increase the volume of the deeper subsurface, residence times, and concentrations of CO₂ and CH₄ in subsurface lateral inflows (as we documented over a single summer), it will also likely lead to fewer in-stream stratification events.

8.0 REFERENCES

- Altor, A.E. and W.J. Mitsch (2006), Methane flux from created riparian marshes: Relationship to intermittent versus continuous inundation and emergent macrophytes, *Ecological Engineering*, 28, 224-234.
- Aufdenkampe, A.K., E. Mayorga, P.A. Raymond, J.M. Melack, S.C. Doney, S.R. Alin, R.E. Aalto, and K. Yoo (2011), Riverine coupling of biogeochemical cycles between land, oceans, and atmosphere, *Frontiers in Ecology and Environment*, 9, 53-60.
- Bastviken, D., J. Cole, M. Pace, and L. Tranvik (2004), Methane emissions from lakes: Dependence of lake characteristics, two regional assessments, and a global estimate, *Global Biogeochemical Cycles*, 18, GB409.

- Berner, R.A. 1980. Early diagenesis: A theoretical approach. Princeton University Press.
- Broecker, W.S. and T.H. Peng (1974), Gas exchange rates between air and sea, *Tellus*, 26(1-2), 21-35.
- Butman, D. and P.A. Raymond (2011), Significant efflux of carbon dioxide from streams and rivers in the United States, *Nature Geoscience*, 4(12), 839-842.
- Cherry, J.E., S.J. Dery, Y. Cheng, M. Stieglitz, A.S. Jacobs, and F. Pan (2014), Climate and hydrometeorology of the Toolik Lake Region and the Kuparuk River Basin: Past, present, and future, In *Alaska's changing Arctic: Ecological consequences for tundra, streams, and lakes (Long-term ecological research)*, eds. G.W. Kling and J.E. Hobbie, 21-60.
- Christensen, T.R. (1993), Methane emission from Arctic tundra, *Biogeochemistry*, 21, 117-139.
- Clymo, R.S. (1984), The limits to peat bog growth, *Philosophical Transactions of the Royal Society of London Series B, Biological Sciences*, 303, 605.
- Cole, J.J. and N.F. Caracao (1998), Atmospheric exchange of carbon dioxide in a low-wind oligotrophic lake measured by the addition of SF₆, *Limnology and Oceanography*, 43(4), 647-656.
- Cory, R.M., B.C. Crump, J.A. Dobkowski, and G.W. Kling (2013), Surface exposure to sunlight simulates CO₂ release from permafrost soil C in the Arctic, *Proceedings of the National Academy of Sciences*, 110(9), 3429-3434.
- Cory, R.M., M.P. Miller, D.M. McKnight, J.J. Guerard, and P.L. Miller (2010), Effect of instrument-specific response on the analysis of fulvic acid spectra, *Limnology and Oceanography—Methods*, 8, 67-78.
- Crawford, J.T., R.G. Striegl, K.P. Wickland, M.M. Dornblaser, and E.H. Stanley (2013), Emissions of

carbon dioxide and methane from a headwater stream network of interior Alaska, *Journal of Geophysical Research—Biogeosciences*, 118, 482-494.

Crump, B.C., G.W. Kling, M. Bahr, and J.E. Hobbie (2003), Bacterioplankton community shifts in an Arctic lake correlate with seasonal changes in organic matter source, *Applied and Environmental Microbiology*, 69(4), 2253-2268.

Crusius, J. and R. Wanninkhof (2003), Gas transfer velocities measured at low wind speed over a lake, *Limnology and Oceanography*, 48(3), 1010-1017.

Eugster, W., G.W. Kling, T. Jonas, J.P. McFadden, A. Wuest, S. MacInyre, and F.S. Chapin (2003), CO₂ exchange between air and water in an arctic Alaskan and midlatitude Swiss lake: Importance of convective mixing, *Journal of Geophysical Research*, 108, D12.

Euskirchen, S. E., A. D. McGuire, and F. S. Chapin, III, (2007), Energy feedbacks of northern high-latitude ecosystems to the climate system due to reduced snow cover during 20th century warming, *Global Change Biology*, 13, 2425–2438.

Freeman, C., N. Fenner, N.J. Ostle, H. Kang, D.J. Dowrick, B. Reynolds, M.A. Lock, D. Sleep, S. Hughes, and J. Hudson (2004), Export of dissolved organic matter from peatlands under elevation carbon dioxide levels, *Nature*, 430(8), 195-198.

Gupta, R.S. (2007), *Hydrology and hydraulic systems*, 3rd ed., Waveland Press, Inc., Long Grove, IL.

Harper, J.R. and W.J. Wiseman, Jr. (1977), Temporal variation of surface roughness over a tundra surface, *Journal of Geophysical Research*, 82(24), 3495-3497.

Helms, J.R., A. Stubbins, J.D. Ritchie, E.C. Minor, D.J. Kieber, and K. Mopper (2008), Absorption

spectral slopes and slope ratios as indicators of molecular weight, source, and photobleaching of chromophoric dissolved organic matter, *Limnology and Oceanography*, 53(3), 955-969.

Hinzman, L.D., D.L. Kane, R.E. Gieck, and K.R. Everett (1991), Hydrologic and thermal properties of the active layer in the Alaska Arctic, *Cold Regions Science and Technology*, 19, 95-110.

Hope, D., S.M. Palmer, M.F. Billet, and J.J.C. Dawson (2004), Variations in dissolved CO₂ and CH₄ in a first-order stream and catchment: An investigation of soil-stream linkages, *Hydrological Processes*, 18(17), 3255-3275.

Hope, D., S.M. Palmer, M.F. Billett, and J.T.C. Dawson (2001), Carbon dioxide and methane from a temperate peatland stream, *Limnology and Oceanography*, 46(4), 847-857.

Humborg, C., C.M. Morth, M. Sundbom, H. Borg, T. Blenckner, R. Giesler, and V. Ittekkot (2010), CO₂ supersaturation along the aquatic conduit in Swedish watersheds as constrained by terrestrial respiration, aquatic respiration and weathering, *Global Change Biology*, 16(7), 1966-1978.

Huttunen, J.T., T.S. Vaisanen, S.K. Hellsten, and P.J. Martikainen (2006), Methane fluxes at the sediment-water interface in some boreal lakes and reservoirs, *Boreal Environment Research*, 11, 27-34.

Irons, J.G. III and M.W. Oswood (1992), Seasonal temperature patterns in an arctic and two subarctic Alaskan (USA) headwater streams, *Hydrobiologia*, 237(3), 147-157.

Jones, J.B. and P.J. Mulholland (1998), Methane input and evasion in a hardwood forest stream: Effects of subsurface flow from shallow and deep pathways, *Limnology and Oceanography*, 43(6), 1243-1250.

- Jonsson, A., G. Algesten, A.K. Bergstrom, K. Bishop, S. Sobek, L. Tranvik, and M. Jansson (2007), Integrating aquatic carbon fluxes in a boreal catchment carbon budget, *Journal of Hydrology*, 334(1-2), 141-150.
- Judd, K.E. and G.W. Kling (2002), Production and export of dissolved C in arctic tundra mesocosms: The roles of vegetation and water flow, *Biogeochemistry*, 60, 213-234.
- Kling, G.W., G.W. Kipphut, M.M. Miller, and W.J. O'Brien (2000), Integration of lakes and streams in a landscape perspective: The importance of material processing on spatial patterns and temporal coherence, *Freshwater Biology*, 43, 477-497.
- Kling, G.W., G.W. Kipphut, and M.C. Miller (1991), Arctic lakes and streams as gas conduits to the atmosphere: Implications for tundra carbon budgets, *Science*, 251(4991), 298-301.
- Knighton, A.D. (1998), *Fluvial forms and processes: A new perspective*, Arnold, London.
- Kirillin, G., H.P. Grossart, and K.W. Tang (2012), Modeling sinking rate of zooplankton carcasses: Effects of stratification and mixing, 57(3), 881-894.
- Martineau, C., Y. Pan, L. Bodrossy, E. Yergeau, L.G. Whyte, and C.W. Greer (2014), Atmospheric methane oxidizers are present and active in Canadian high Arctic soils, *FEMS Journal of Microbiology*, doi:10.1111/1574-6941.12287.
- MacIntyre, S., A. Jonsson, M. Jansson, J. Aberg, D.E. Turney, and S.D. Miller (2010), Buoyancy flux, turbulence, and gas transfer coefficient in a stratified lake, *Geophysical Research Letters*, 37, L24604.
- McGuire, A.D., L.G. Anderson, T.R. Christensen, S. Dallimore, L. Guo, D.J. Hayes, M. Heimann, T.D. Lorenson, R.W. MacDonald, and N. Roulet (2009), *Ecological Monographs*, 79(4), 523-555.

- McKnight, D.M., E.W. Boyer, P.K. Westerhoff, P.T. Doran, T. Kulbe, and D.T. Anderson (2001), Spectrofluorometric characterization of dissolved organic matter for indication of precursor organic material and aromaticity, *Limnology and Oceanography*, 46(1), 38-48.
- McNamara, J.P., D.L. Kane, and L.D. Hinzman (1998), An analysis of streamflow hydrology in the Kuparuk River Basin, arctic Alaska: A nested watershed approach. *Journal of Hydrology*, 206(1-2), 39-57.
- Merck, M.F., B.T. Neilson, R.M. Cory, and G.W. Kling (2012), Variability of in-stream and riparian storage in a beaded arctic stream, *Hydrological Processes*, 26, 2938-2950.
- Mulholland, P. (1993), Hydrometric and stream chemistry evidence of three storm flowpaths in Walker Branch Watershed, *Journal of Hydrology*, 151, 129-316.
- Natural Resources Conservation Service (NRCS; 2013), Alaska SNOTEL Sites—Imnavait Creek, retrieved April 11, 2014 from <http://www.wcc.nrcs.usda.gov/nwcc/site?sitenum=968&state=ak>.
- Neu, V., C. Neill, and A.V. Krusche (2011), Gaseous and fluvial carbon export from an Amazon forest watershed, *Biogeochemistry*, 105, 133-147.
- Page, S.E., J.R. Logan, R.M. Cory, and K. McNeill (2014), Evidence for dissolved organic matter as the primary source and sink of photochemically produced hydroxyl radical in arctic surface waters (2014), *Environmental Science—Processes and Impacts*, 4, 807-822.
- Page, S.E., G.W. Kling, M. Sander, K.H. Harrold, J. R. Logan, K. McNeill, and R.M. Cory (2013), Dark formation of hydroxyl radical in arctic soil and surface waters, *Environmental Science and Technology*, 47, 12860-12867.
- Peterson, B.J., J.E. Hobbie, and T.L. Corliss (1986), Carbon flow in a tundra stream ecosystem, *Canadian Journal of Fisheries and Aquatic Sciences*, 23, 1259-1270.
- Polyakov, I. D., G. V. Alekseev, R. V. Bekryaev, U. Bhatt, R. Colony, M. A. Johnson, V. P. Karklin, A.

- P. Makshtas, D. Walsh, and A. V. Yulin (2002), Observationally based assessment of polar amplification of global warming, *Geophysical Research Letters*, 29, 1878.
- Raymond, P.A., J. Hartmann, R. Lauerwald, S. Sobek, C. McDonald, M. Hoover, D. Butman, R. Striegel, E. Mayorga, C. Humborg, P. Kortelainen, H. Durr, M. Meybeck, P. Ciais, and P. Guth (2013), Global carbon dioxide emissions from inland waters, *Nature*, 503, 355-359.
- Raymond, P.A., C.J. Zappa, D. Butman, T.L. Bott, J. Potter, P. Mulholland, A.E. Laursen, W.H. McDowell, and D. Newbold (2012), Scaling the gas transfer velocity and hydraulic geometry in streams and small rivers, *Limnology and Oceanography—Fluids and Environments*, 2, 41-53.
- Schiff, S., R. Aravena, E. Mewhinney, R. Elgood, B. Warner, P. Dillon, and S. Trumbore (1998), Precambrian shield wetlands: Hydrologic control of the sources and export of dissolved organic matter, *Climatic Change*, 40, 167-188.
- Schubert, C.J., T. Diem, and W. Eugster (2012), Methane emissions from a small wind shielded lake determined by eddy covariance, flux chambers, anchored funnels, and boundary layer model calculations: A comparison, *Environmental Science and Technology*, 46(8), 4515-4522.
- Schwarzenbach, R.P., P.M. Gschwend, and D.M. Imboden (2002), *Environmental Organic Chemistry*, John Wiley and Sons, Inc., Hoboken, NJ.
- Serreze, M. C. and J. A. Francis (2006), The Arctic amplification debate, *Climatic Change*, 76, 241–264.
- Sweerts, J.R.A., M. Bar-Gilissen, A.A. Cornelese, and T.E. Cappenberg (1991), Oxygen-consuming processes at the profundal and littoral sediment-water interface of a small meso-eutrophic lake (Lake Vecten, The Netherlands), *Limnology and Oceanography*, 36(6), 1124-1133.
- Tarnocai, C., J.G. Canadell, E.A.G. Schuur, P. Kuhry, G. Mazhitova, and S. Zimov (2009), Soil organic

carbon pools in the northern circumpolar permafrost region, *Global Biogeochemical Cycles*, 23, GB2023.

Taylor, J.R. (1997), *Introduction to error analysis*, University Science Books, Sausalito, CA.

Teodoru, C.R., P.A. del Giorgio, Y.T. Prairie, and M. Camire (2009), Patterns in pCO₂ in boreal streams and rivers of northern Quebec, Canada, *Global Biogeochemical Cycles*, 23(2), 1-11.

Vachon, D., Y.T. Prairie, and J.J. Cole (2010), The relationship between near-surface turbulence and gas transfer velocity in freshwater systems and its implications for floating chamber measurements of gas exchange, *Limnology and Oceanography*, 55(4), 1723-1732.

Walker, D.A. and H.A. Maier, 2008, "Vegetation in the vicinity of Toolik Field Station, Alaska, *Biological Papers of the University of Alaska*, 28, Institute of Arctic Biology, Fairbanks, AK.

Walker, D.A., N.D. Lederer, and M.D. Walker, 1987, Permanent vegetation plots: Site factors, soil physical and chemical properties and plant species cover, Department of Energy R4D Program, Institute of Arctic and Alpine Research, University of Colorado, Boulder, CO.

Wanninkhof, R. (1992), Relationship between wind speed and gas exchange over the ocean, *Journal of Geophysical Research*, 97, 7373-7382.

Ward, C.P., R.L. Sleighter, P.G. Hatcher, and R.M. Cory (2014), Insights into the complete and partial photooxidation of black carbon in surface waters, *Environmental Science—Processes and Impacts*, DOI:10.1039/c3em00597f.

Weishaar, J.L., G.R. Aiken, B.A. Bergamaschi, M.S. Fram, R. Fuji, and K. Mopper (2003), Evaluation of specific absorbance as an indicator of the chemical composition and reactivity of dissolved organic carbon, *Environmental Science and Technology*, 37, 4702-4708.

Wilhelm, E., R. Battino, and R.J. Wilcock (1977), Low-pressure solubility of gases in liquid water, Chemical Reviews, 77(2), 219-262.

Zarnetske, J.P., M.N. Gooseff, W.B. Bowden, M.J. Greenwald, T.R. Brosten, J.H. Bradford, and J.P. McNamara (2007), Influence of morphology and permafrost dynamics on hyporheic exchange in arctic headwater streams under warming climate conditions, Geophysical Research Letters, 35, L02501.

9.0 APPENDIX A

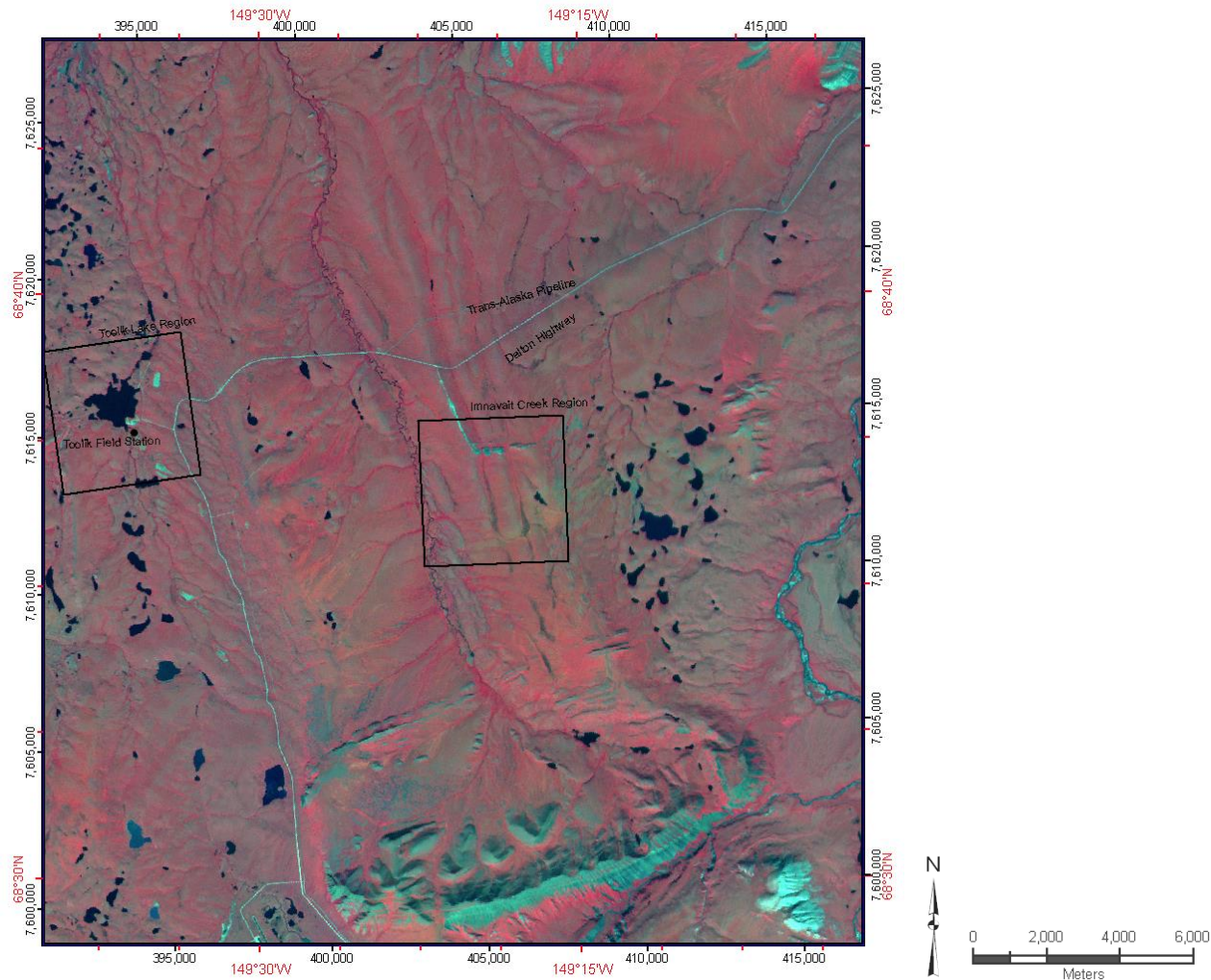


Figure A1. False color image of the Innavait Creek Region relative to the Toolik Lake Region and the Kuparuk River. Innavait Creek flows into the Kuparuk River, which flows into the Arctic Ocean near Prudhoe Bay. The large land surface area covered by headwater streams in this area of the North Slope can be seen in this image, from Walker and Maier (2008).

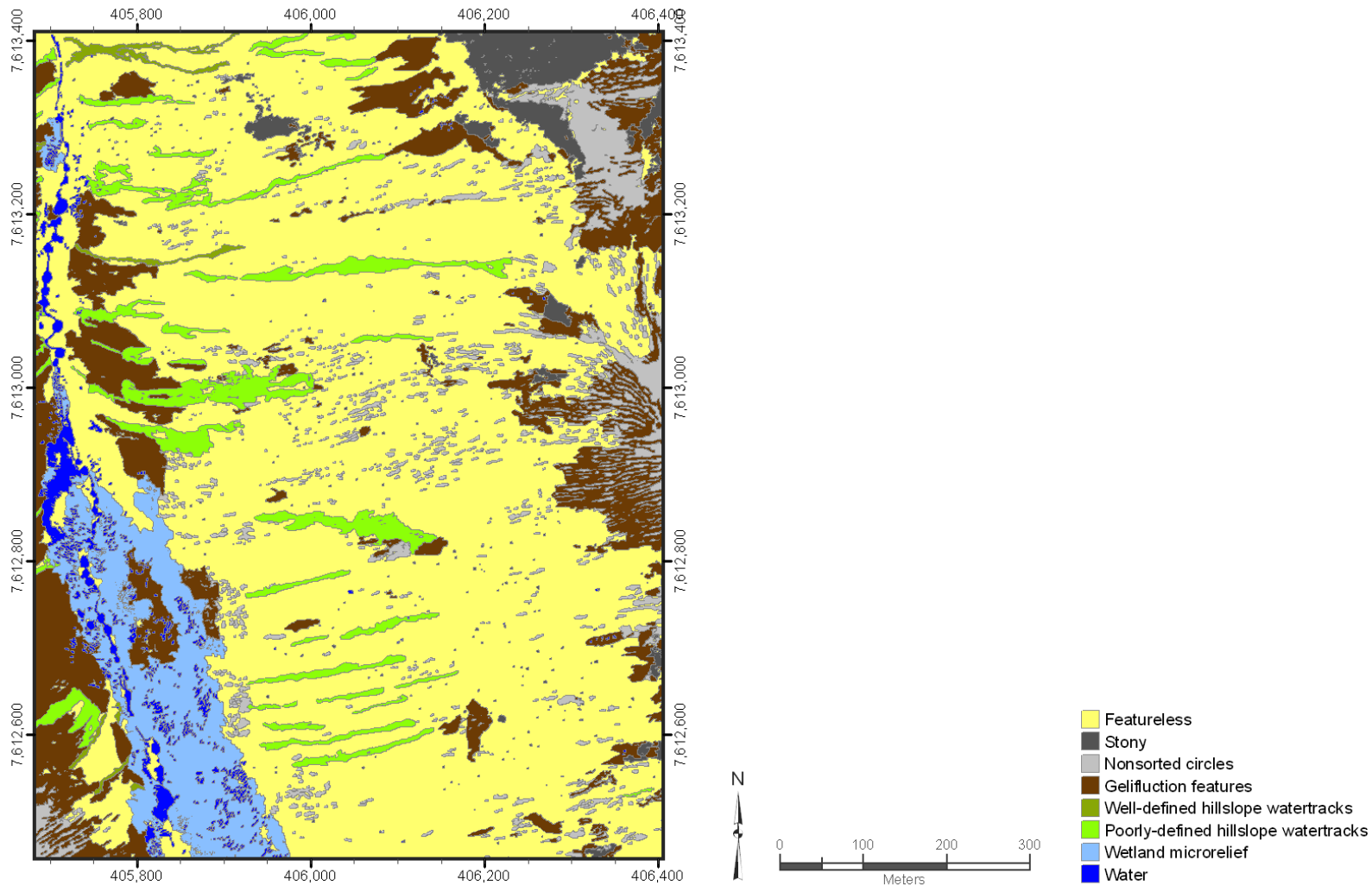


Figure A2. Surficial Geomorphology of Innavaik Creek. The spatial extent of riparian wetlands at Innavaik is highlighted next to beaded pools. Hill slope water tracks are also highlighted in this image, from (Walker et al., 1987).

10.0 APPENDIX B

Surface inflow—The flume was calibrated using measured discharge and a pressure transducer. Stage height in an attached stilling well, which was determined using and a non-vented pressure transducer (Level Troll 500, In-Situ Inc.), was related to discharge, or inflow into Pool 2. Stage height, h (m), was obtained from pressure, P (Pa), in the following relationship:

$$h = \frac{P}{\rho g} \quad (\text{B1})$$

where ρ is the density of water (kg m^{-3}) and g is standard gravity (m s^{-2}). Atmospheric pressure (Baro Troll, In-Situ Inc.) was subtracted from total pressure to obtain P .

Subsurface lateral inflows—Subsurface discharge, Q (L d^{-1}), perpendicular to Pools 2 and 3 from the east and west riparian wetlands were estimated using differences between water elevations within piezometers installed in the wetlands and water elevations within Pools 2 and 3, according to Darcy's Law:

$$Q = A k \frac{dH}{dx} \quad (\text{B2})$$

where A is the vertical cross-sectional area between piezometers (m^2) perpendicular to Q , k is the hydraulic conductivity of the soil at a given depth (cm s^{-1}), dH is difference between piezometer and pool water elevation (hydraulic head; m), and dx (m) is the distance between the piezometer and the pool. Water elevation in each piezometer was determined by GPS (surveying elevation (m above sea level, Alaska GEOID09; Trimble S3 Servo-Autolock-Robotic Total Station) at the top of each well casing, subtracting the length of that well casing (162.5 cm), and adding water depth to pressure transducer diaphragm (stage height). Pressure transducer diaphragms were positioned 2.5 cm from the bottom of the well, and piezometer water elevations were further corrected for this. Stage height was measured both manually and by using Aqua Troll 200 (In-Situ Inc.) non-vented pressure transducers. Pool stage heights were measured (vented 600LS sonde, YSI) and pool water elevations were surveyed in Pools 2 and 3 on August 3. This relationship between continuous pressure measurements and surface water elevation from GPS was used to extrapolate pool water elevation from stage height on other dates.

Error propagation—Following Taylor (1997), if $x + y = q$, then the error or uncertainty ($\hat{\sigma}$) associated with x (δx) and y (δy) propagated to q is the sum of these uncertainties, represented as:

$$\delta q = \sqrt{(\delta x)^2 + (\delta y)^2} \quad (\text{B9})$$

If $x * y$ or $x / y = q$, then the error or uncertainty propagated to q is the sum of the fractional uncertainties associated with x ($\delta x / x$) and y ($\delta y / y$), represented as:

$$\frac{\delta q}{|q|} = \sqrt{\left(\frac{\delta x}{|x|}\right)^2 + \left(\frac{\delta y}{|y|}\right)^2} \quad (\text{B10})$$

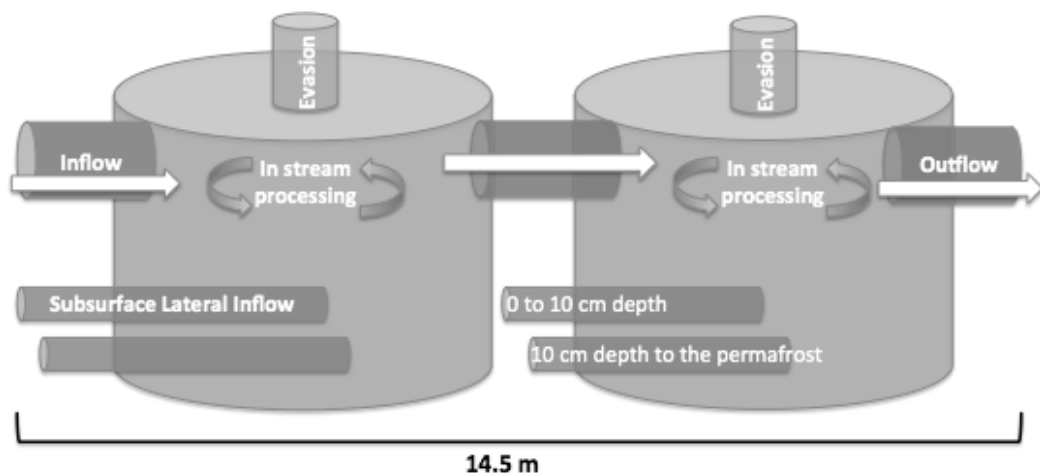


Figure B1. Diagram of carbon mass balances for the study reach. CO_2 and CH_4 within subsurface lateral inflows from riparian wetlands to Innavait were measured at 0 to 10 cm depth and 10 cm depth to the permafrost boundary on the east and west banks of each pool.

11.0 APPENDIX C

Table C1. Summary of water balances by pool and combined as a reach on July 4, July 16, and July 31. Reach-scale terms in the water balances were determined by adding terms for Pools 2 and 3. In addition to surface inflows and processes (i.e., precipitation and evaporation), subsurface lateral inflows are included for riparian wetlands on the east and west bank of Innvait Creek at 0 to 10 cm depth and at 10 cm depth to the permafrost boundary.

<i>Surface (L/h)</i>	4-Jul			16-Jul			31-Jul		
	<i>POOL 2</i>	<i>POOL 3</i>	<i>REACH</i>	<i>POOL 2</i>	<i>POOL 3</i>	<i>REACH</i>	<i>POOL 2</i>	<i>POOL 3</i>	<i>REACH</i>
Surface Inflow	120000.0	120047.7		6900.0	6997.8		72000	72052.2	
Precipitation	0.0	0.0	0.0	0.0	0.0	0.0	0.0	0.0	0.0
Evaporation	0.1	0.1	0.3	0.3	0.3	0.7	0.1	0.1	0.2
Net Surface Inflow	119999.9	120047.5	120068.3	6899.7	6997.5	7047.2	71999.9	72052.1	72088.9
<i>Subsurface (L/h)</i>									
0-10 cm East	11	4.6	15.1	27	12.6	39.9	10	8.1	17.9
10 cm-Permafrost East	12	6.2	18.6	30	23.1	53.1	19	15.5	34.9
0-10 cm West	10	5	14	16	6	22	8	5	13
10 cm-Permafrost West	15	5	21	25	8	33	15	8	23
Net Subsurface Inflow	48	20.8	68.6	98	49.8	147.9	52	36.8	89.2
<i>Percent Total Inflow</i>	0.04	0.02	0.06	1.42	0.71	2.10	0.07	0.05	0.12
<i>Net Outflow</i>	120047.7	120068.3	120068.3	6997.8	7047.2	7047.2	72009.2	72088.9	72088.9

Table C2. Subsurface lateral inflows, per cm of soil depth, for riparian wetlands on the east and west bank of Imnavait Creek at 0 to 10 cm depth and at 10 cm depth to the permafrost boundary on July 4, July 16, and July 31.

<i>Subsurface (L/h/cm)</i>	4-Jul			16-Jul			31-Jul		
	<i>POOL 2</i>	<i>POOL 3</i>	<i>REACH</i>	<i>POOL 2</i>	<i>POOL 3</i>	<i>REACH</i>	<i>POOL 2</i>	<i>POOL 3</i>	<i>REACH</i>
0-10 cm East	1.1	0.5	1.5	3	1	4	1.0	0.8	1.8
10 cm-Permafrost East	0.3	0.2	0.5	0.6	0.5	1.1	0.3	0.3	0.6
0-10 cm West	1.0	1.0	2.0	1.6	0.6	2.2	0.8	0.5	1.3
10 cm-Permafrost West	0.3	0.1	0.5	0.5	0.2	0.7	0.3	0.1	0.4

Table C3. Residence times (min) calculated for subsurface lateral inflows at 0 to 10 cm depth and at 10 cm depth to permafrost boundary beneath riparian wetlands on the east and west bank of Imnavait Creek.

	Residence Times (min)					
	4-Jul-2013	5-Jul-2013	16-Jul-2013	26-Jul-2013	31-Jul-2013	3-Aug-2013
Pool 2 East						
Pool 2 East 0 -10 cm	97	97	37	46	105	60
Pool 2 East 10 cm-Permafrost	2130	2130	1067	796	1872	1237
Pool 2 West						
Pool 2 West 0 -10 cm	113	113	70	96	137	102
Pool 2 West 10 cm-Permafrost	2056	2056	1453	1778	2594	1854
Pool 3 East						
Pool 3 East 0 -10 cm	277	277	101	96	156	88
Pool 3 East 10 cm-Permafrost	5137	5137	1741	2021	3155	2011
Pool 3 West						
Pool 3 West 0 -10 cm	233	233	175	198	207	152
Pool 3 West 10 cm-Permafrost	4741	4741	3765	4758	4659	3852

12.0 APPENDIX D

Table D1. DOC mass balances by pool and combined as a reach during July 26 July 31-August 3. Reach-scale terms in the C mass balances were determined by adding terms for Pools 2 and 3. DOC within subsurface lateral inflows draining riparian wetlands on the west bank of Imnavait Creek is included (subsurface), both at the shallow and deeper layer. Using the change in mg DOC h⁻¹ per m of stream length, expected mass at Imnavait Weir—0.7 km downstream from Pool 3—was calculated.

<i>Surface (mg DOC/h)</i>	26-Jul-2013			31-Jul-2013 to 3-Aug-2013		
	<i>POOL 2</i>	<i>POOL 3</i>	<i>REACH</i>	<i>POOL 2</i>	<i>POOL 3</i>	<i>REACH</i>
Surface Inflow	54000			35000	35043	
<i>Subsurface (mg/h)</i>						
0-10 cm West	14.1	14.4	28.5	19	16	35
10 cm-Permafrost West	33	19	52.4	24	23	47
Net Subsurface Inflow	47.1	33.8	80.9	43	40	82
<i>Percent Total Inflow</i>	0.09	0.06	0.15	0.12	0.11	0.235
<i>Expected Net Outflow</i>			54081			35082
<i>Observed Net Outflow</i>			53000			36000
<i>Change in C per h</i>			-1000			1000
<i>Change in C per h per m Stream Length</i>			-69			69
<i>Imported:Exported</i>			1.02			0.97
<i>Expected Weir Inflow</i>			-46326			46326
<i>Observed Weir Inflow</i>			1067398			183096

Table D2. CO₂ within subsurface lateral inflows through each cm of the shallow and deeper layers of riparian wetlands on the east and west bank of Innavait Creek during July 4-5, July 26, and July 31-August 3.

<i>Subsurface (mg CO₂-C/h/cm)</i>	4-Jun to 5-Jun			26-Jul			31-Jul to 3-Aug		
	<i>POOL 2</i>	<i>POOL 3</i>	<i>REACH</i>	<i>POOL 2</i>	<i>POOL 3</i>	<i>REACH</i>	<i>POOL 2</i>	<i>POOL 3</i>	<i>REACH</i>
0-10 cm East	1.82±0.01	5.2±0.1		13.1±0.3	15.0±0.4		4.18±0.02	8.0±0.9	
10 cm-Permafrost East	1.96±0.01	0.858±0.001		18.1±0.4	4.5±0.1		7.8±0.2	3.00±0.04	
0-10 cm West	9.0±0.1	31.6±0.6		7.7±0.1	14.2±0.4		9.4±0.6	8±1	
10 cm-Permafrost West	3.21±0.07	6.9±0.2		3.72±0.02	4.2±0.1		3.6±0.1	3.47±0.03	

Table D3. CH₄ within subsurface lateral inflows through each cm of the shallow and deeper layers of riparian wetlands on the east and west bank of Innavait Creek during July 4-5, July 26, and July 31-August 3.

<i>Subsurface (mg CH₄-C/h/cm)</i>	4-Jun to 5-Jun			26-Jul			31-Jul to 3-Aug		
	<i>POOL 2</i>	<i>POOL 3</i>	<i>REACH</i>	<i>POOL 2</i>	<i>POOL 3</i>	<i>REACH</i>	<i>POOL 2</i>	<i>POOL 3</i>	<i>REACH</i>
0-10 cm East	0.09±0.01	0.52±0.03		0.48±0.02	0.96±0.03		0.04±0.03	0.32±0.05	
10 cm-Permafrost East	0.152±0.002	0.096±0.002		1.10±0.02	0.45±0.01		0.49±0.02	0.26±0.01	
0-10 cm West	0.070±0.002	2.03±0.07		0.13±0.01	0.73±0.01		0.68±0.04	0.46±0.05	
10 cm-Permafrost West	0.29±0.01	0.33±0.03		0.180±0.003	0.186±0.002		0.27±0.05	0.192±0.001	

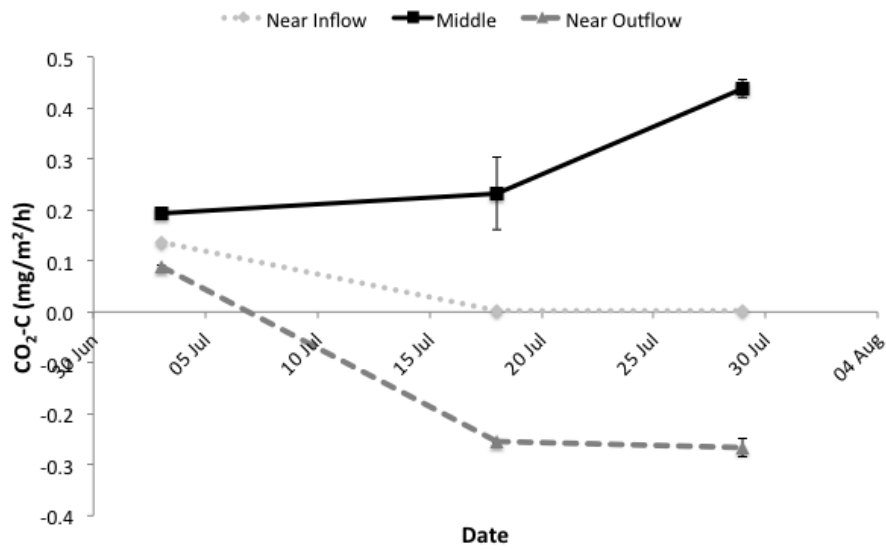


Figure D1. Hyporheic flux of CO₂ near the inflow ($n=3$ replicate samples), middle ($n=3$), and outflow ($n=3$) of Pool 6 on July 3, July 18, and July 29. Error bars represent the standard error associated with each mean ($n=3$). Fluxes near the outflow are negative (influxes), perhaps indicating that dilute surface water with lower concentrations of CO₂ is being forced into the hyporheic zone by stream velocities accelerating across sediments as water enters the chute to Pool 7. CO₂ fluxes are always greatest in the middle of Pool 6, suggesting deposition and respiration of larger amounts of OM here. When converted to g and scaled to sediment surface area in Pools 2 and 3, hyporheic flux of CO₂ is a negligible term in C mass balances.

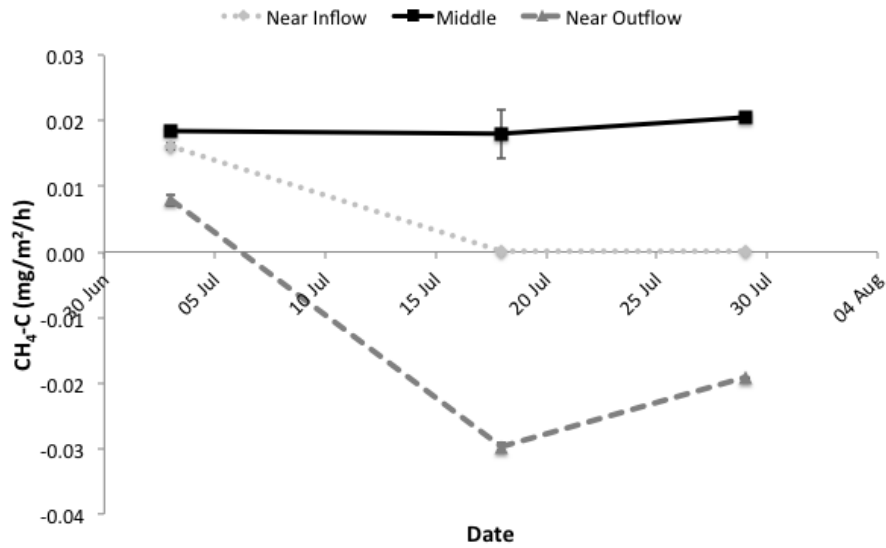


Figure D2. Hyporheic flux of CH₄ near the inflow ($n=3$ replicate samples), middle ($n=3$), and outflow ($n=3$) of Pool 6 on July 3, July 18, and July 29. Error bars represent the standard error associated with each mean ($n=3$). Fluxes near the outflow are negative (influxes), perhaps indicating that dilute surface water with lower concentrations of CH₄ is being forced into the hyporheic zone by stream velocities accelerating across sediments as water enters the chute to Pool 7. CH₄ fluxes are always greatest in the middle of Pool 6, suggesting deposition and respiration of larger amounts of OM here. When converted to g and scaled to sediment surface area in Pools 2 and 3, hyporheic flux of CH₄ is a negligible term in C mass balances.

13.0 APPENDIX E

Table E1. Concentrations of CO₂ (mg C L⁻¹) measured in the epilimnion (*n*=6) and within riparian soil waters in dry (*n*=6) and inundated (*n*=6) areas of the wetlands located 1 m (*n*=12) and 6 m (*n*=12) from the stream edge, during June 26 (Figure 2). Standard errors associated with each mean are included. Concentrations of CO₂ are significantly greater in dry areas (*p*=0.001).

	CO ₂ -C (mg/L)				
	1 m		6 m		Epilimnion
	Wet	Dry	Wet	Dry	
<i>June 26</i>	5.3±0.2	14.4±6	8±2	11±1	1.77±0.02

Table E2. Concentrations of CH₄ (mg C L⁻¹) measured in the epilimnion (*n*=6) and within riparian soil waters in dry (*n*=6) and inundated (*n*=6) areas of the wetlands located 1 m (*n*=12) and 6 m (*n*=12) from the stream edge, during June 26. Standard errors associated with each mean are included. Concentrations of CH₄ are significantly greater in dry areas (*p*=0.05).

	CH ₄ -C (mg/L)				
	1 m		6 m		Epilimnion
	Wet	Dry	Wet	Dry	
<i>June 26</i>	0.21±0.01	0.9±0.1	0.4±0.1	0.4±0.2	0.031±0.002

Table E3. Concentrations of CO₂ (mg C L⁻¹) measured in the epilimnion (*n*=6) and within riparian soil waters at 0 to 10 cm depth (*n*=6) and at 10 cm depth to the permafrost boundary (*n*=6), in dry (*n*=12) and inundated (*n*=12) areas of the wetlands located 1 m (*n*=24) and 6 m (*n*=24) from the stream edge. Standard errors associated with each mean are included. Concentrations of CO₂ were significantly greater in dry areas than in wet areas during July 9 (*p*=0.003) and August 1 (*p*=0.02). Concentrations of CO₂ were also significantly greater at 10 cm depth to the permafrost boundary during July 9 (*p*<0.001) and August 1 (*p*=0.05).

	CO ₂ -C (mg L ⁻¹)										Epilimnion
	1 m				6 m				Water Track		
	Wet		Dry		Wet		Dry		10 cm	25 cm	
	10 cm	25 cm	10 cm	25 cm	10 cm	25 cm	10 cm	25 cm			
July 9	8±1	16±1	22±2	30.5±0.6	9.4±0.3	23±2	13.2±0.9	24.3±0.4			1.43±0.01
August 1	3.5±0.5	17.5±3.5	30±1	29±1	14±3	19±4	11±1	32.0±0.6	13.1±0.4	24.2±0.3	1.14±0.03

Table E4. Concentrations of CH₄ (mg C L⁻¹) measured in the epilimnion (*n*=6) and within riparian soil waters at 0 to 10 cm depth (*n*=6) and at 10 cm depth to the permafrost boundary (*n*=6), in dry (*n*=12) and inundated (*n*=12) areas of the wetlands located 1 m (*n*=24) and 6 m (*n*=24) from the stream edge. Standard errors associated with each mean are included. Concentrations of CH₄ were not significantly greater in dry areas than in wet areas during July 9 and August 1. Concentrations of CO₂ were significantly greater at 10 cm depth to the permafrost boundary during July 9 (*p*<0.001) and August 1 (*p*<0.001).

	CH ₄ -C (mg ⁻¹)										Epilimnion
	1 m				6 m				Water Track		
	Wet		Dry		Wet		Dry		10 cm	25 cm	
	10 cm	25 cm	10 cm	25 cm	10 cm	25 cm	10 cm	25 cm			
July 9	0.14±0.02	1.2±0.1	1.0±0.2	1.52±0.05	0.7±0.1	1.37±0.04	0.6±0.1	1.44±0.01			0.023±0.001
August 1	0.06±0.02	1.2±0.2	1.4±0.1	1.52±0.02	0.7±0.1	1.15±0.07	0.7±0.3	1.27±0.04	0.09±0.01	0.032±0.004	0.011±0.002

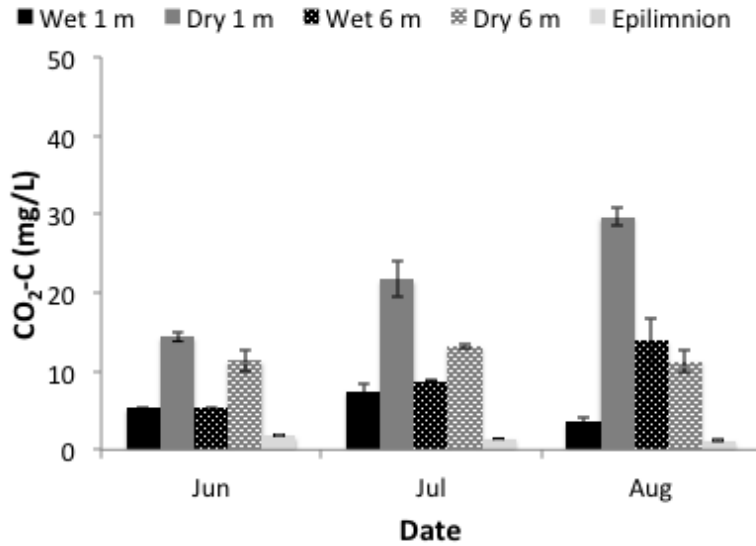


Figure E1. CO₂ concentrations (mg C L⁻¹) in the epilimnion (*n*=6; light grey) and within riparian soil waters at 0 to 10 cm depth in wet (*n*=6; black) and dry (*n*=6; dark grey) areas located 1m (*n*=6) and 6 m (*n*=6) from the pool edge on June 26, July 9, and August 1. Standard errors associated with each mean are included (*n*=2).

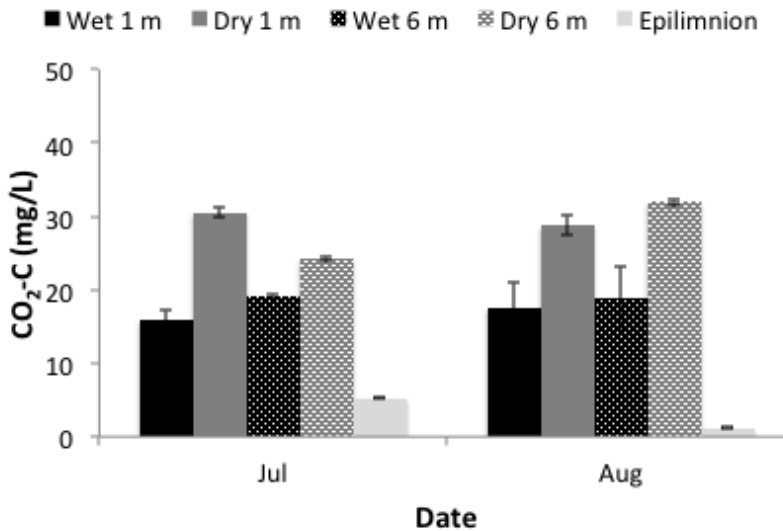


Figure E2. CO₂ concentrations (mg C L⁻¹) in the epilimnion (*n*=6; light grey) and within riparian soil waters at 10 cm depth to the permafrost boundary in wet (*n*=6; black) and dry (*n*=6; dark grey) areas located 1m (*n*=6) and 6 m (*n*=6) from the edge of the stream on June 26, July 9, and August 1. Standard errors associated with each mean are included (*n*=2).

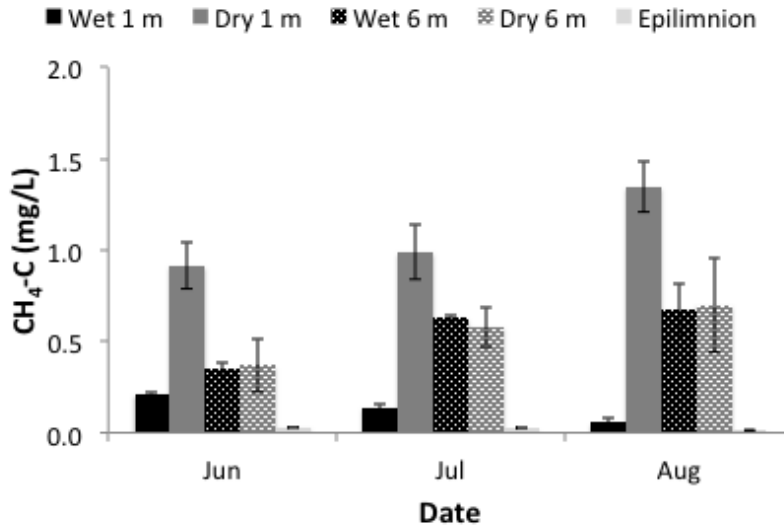


Figure E3. CH₄ concentrations (mg C L⁻¹) in the epilimnion (*n*=6; light grey) and within riparian soil waters at 0 to 10 cm depth in wet (*n*=6; black) and dry (*n*=6; dark grey) areas located 1m (*n*=6) and 6 m (*n*=6) from the edge of the stream on June 26, July 9, and August 1. Standard errors associated with each mean are included (*n*=2).

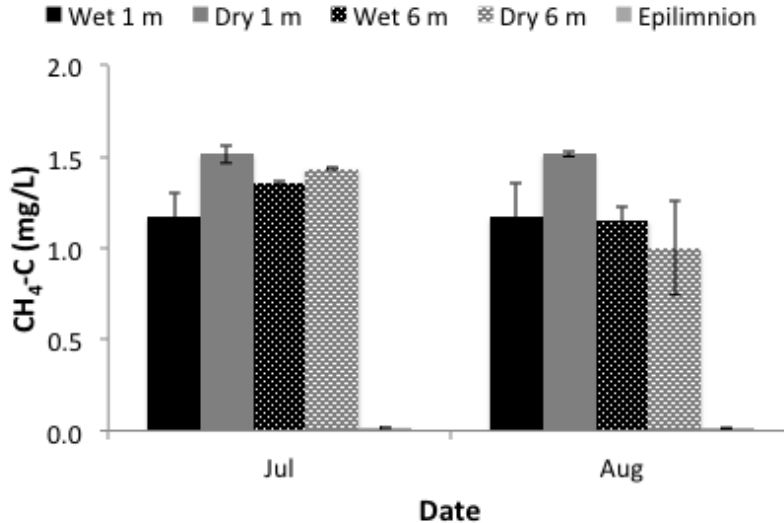


Figure E4. CH₄ concentrations (mg C L⁻¹) in the epilimnion (*n*=6; light grey) and within riparian soil waters at 10 cm depth to the permafrost boundary in wet (*n*=6; black) and dry (*n*=6; dark grey) areas located 1m (*n*=6) and 6 m (*n*=6) from the edge of the stream on June 26, July 9, and August 1. Standard errors associated with each mean are included (*n*=2).

Table E5. CO₂ production within BOD bottles ($\mu\text{mol L}^{-1} \text{h}^{-1} \text{g}^{-1}$) during incubations of soil and sediment and soil and surface water sampled in and near Imnavait Creek, with standard errors associated with each mean included. CO₂ production was normalized to the dry weight (g) of soil and sediment cores when they were included in BOD bottles.

$(\mu\text{m CO}_2 \text{ L}^{-1} \text{ h}^{-1} \text{ g}^{-1})$	Wetland Soil Cores	<i>n</i>
1 m	2.0±0.1	12
6 m	3.3±0.4	12
0-10 cm	4.8±0.7	9
10 cm-Ice	3±1	6
	Wetland Soil Water	<i>n</i>
	0.2±0.1	9
	Hill Slope Soil Cores	<i>n</i>
Water Track	1.7±0.4	6
Organic Layer	1.1±0.2	6
Mineral Layer	0.33±0.04	6
	Pool Sediment Cores	<i>n</i>
Near Inflow	2.7±0.5	6
Middle	7±2	6
Near Outflow	1.5±0.5	5
	Pool Water	<i>n</i>
Epilimnion	0.09±0.01	12
Hypolimnion	0.01±0.01	12

14.0 APPENDIX F

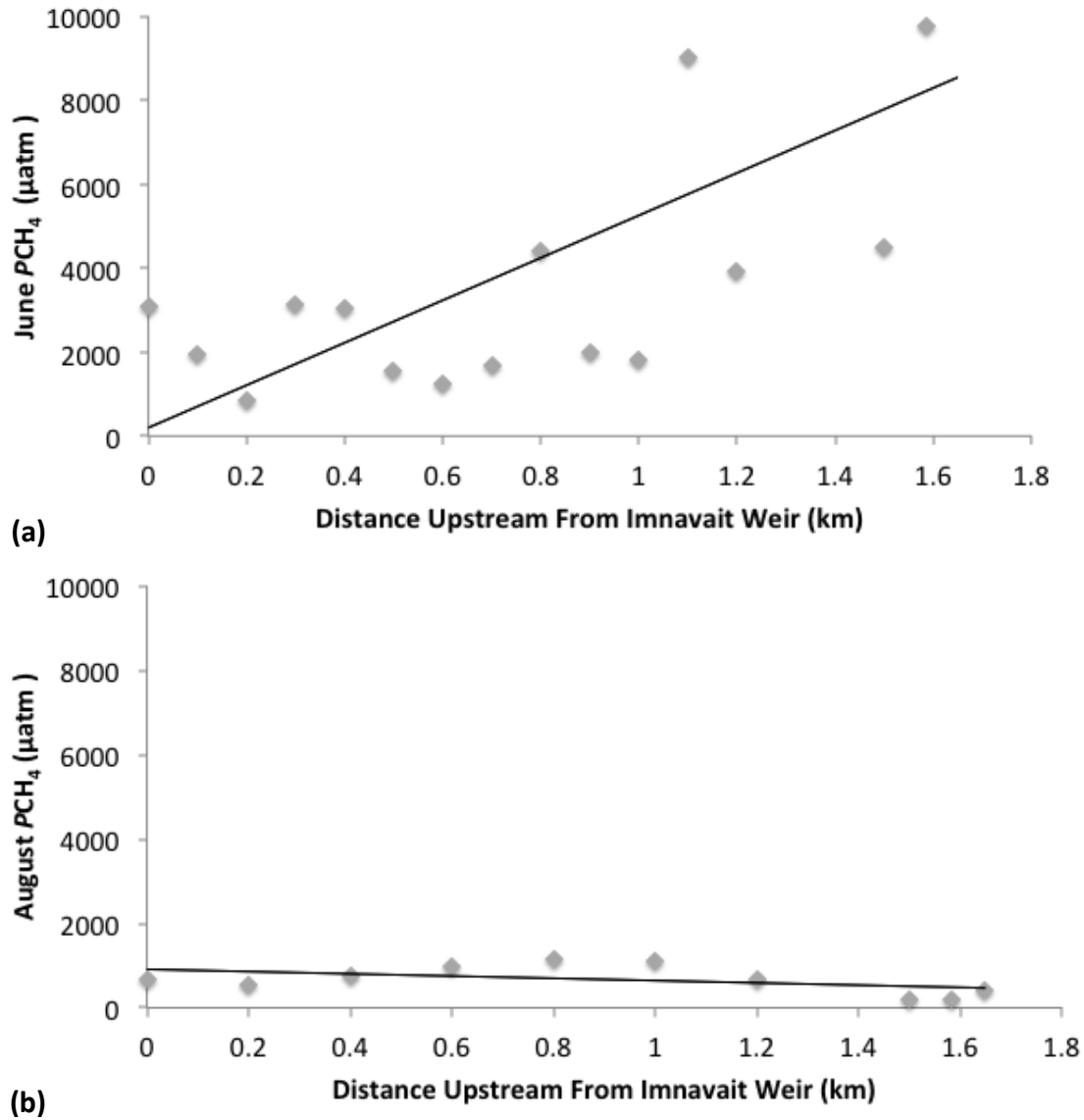


Figure F1. CH_4 (μatm) from Innavait Weir at 0 km to 1.7 km upstream, measured by the Arctic LTER on June 28 (a) and August 8 (b), 2004.

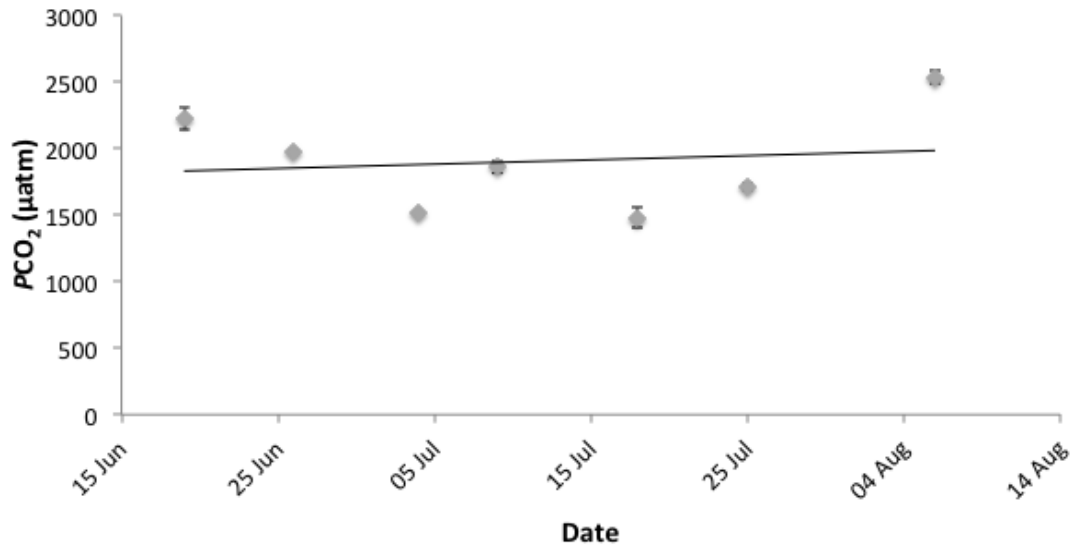


Figure F2. CO₂ (µatm) at Innavait Weir from June 20 to August 6, 2013 ($n=14$). Error bars represent the standard error associated with each mean ($n=2$).